Drag reduction with riblets in nature and engineering

D.W. Bechert & W. Hage
Department of Turbulence Research, German Aerospace Center (DLR), Berlin, Germany.

Abstract

Reduction of wall friction of turbulent boundary layer flows can be achieved by using surfaces with properties that are related to skin structures occurring in nature. The scales of several species of fast-swimming sharks show a tiny ribbed structure. This ribbed structure hampers the momentum exchange at the surface that is the origin of the turbulent shear stress. The drag-reducing mechanism of ribbed surfaces (or riblets) is explained by using an analytical model that defines the viscous region of the flow, where the riblets are completely immersed in the viscous sublayer of the turbulent boundary layer. Wall shear stress reduction has been investigated experimentally for various riblet surfaces including a replica of sharkskin consisting of 800 plastic model scales with compliant anchoring. The application of these types of structure to long-range commercial aircraft is discussed, including the effect of the drag reductions on the operational costs of the aircraft.

1 Introduction

Drag reduction of a moving animal or vehicle can be achieved by a reduction of wall shear stress and, in some situations, by separation control. Here we focus on *turbulent* wall shear stress reduction. Obviously laminar flow, which has been successfully used on glider wings, offers the lowest attainable wall shear stress. On commercial aircraft, however, the problems associated with the implementation of laminar flow on swept transonic wings are at present not yet completely solved. Even when laminar flow is maintained over a major percentage of the wing, most of the aircraft surface will still have a turbulent boundary layer. Turbulent wall shear stress reduction, therefore, remains important in all scenarios of future aircraft design.

1.1 The mechanism of sharkskin or 'riblets'

American scientists invented ribbed surfaces on the basis of fluid-dynamical reasoning, parallel work in Germany was motivated by observations of the structure of sharkskins [1–3]. Sharks, such

WIT Transactions on State of the Art in Science and Engineering, Vol 4, © 2006 WIT Press
www.witpress.com, ISSN 1755-8336 (on-line)
doi:10.2495/1-84564-095-0/5g

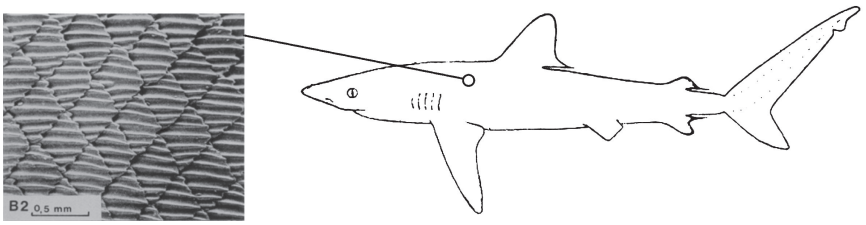

Figure 1: Microstructure of the skin of the Galapagos shark (*Carcharhinus galapagensis*). Photograph by W.E. Reif [4].

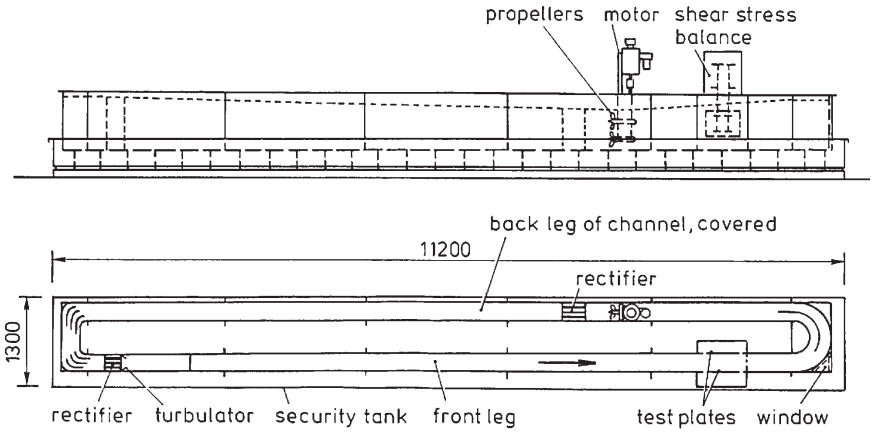

Figure 2: Survey of the Berlin oil channel for drag reduction research.

as the very fast Mako shark (*Isurus oxyrinchus*), operate at comparatively high Reynolds numbers ($\mathrm{Re} \approx 10^6$–10^7). The skins of these sharks exhibit an intriguing microstructure shown in Fig. 1.

The scales of fast sharks are very small, typically one-third of a millimetre. On the scales there are ridges aligned in the flow direction with a lateral distance of roughly 1/20 mm. This observation motivated Reif and Dinkelacker to start experimental studies of this particular type of ribbed surface [2]. The aim was to look for possible drag reduction of a turbulent boundary layer. Walsh in the US, at roughly the same time, reasoned that a ribbed surface could be a promising way of reducing turbulent skin friction [5]. Both groups were able to demonstrate a measurable drag reduction.

Our group entered this field in 1983. At first, we considered it essential to prove by our own measurements that riblets did indeed provide a means of reducing drag. The first step in our investigation was to build a sensitive and accurate shear stress balance for our wind tunnel. This device provided the evidence showing that the turbulent shear stress was reduced by the riblets. Unfortunately the flow conditions in a typical wind tunnel are such that one has to deal with very small ribs with a typical lateral rib spacing of 0.5 mm or less. This small size caused significant production problems in fabricating suitable test surfaces. Finally, we realized that it would take decades to arrive at optimized configurations by experimentation in this facility.

This led us to design a dedicated facility for riblet research: The Berlin oil channel, which is shown in Figs 2 and 3. In this facility a typical lateral rib spacing of 5 mm could be used to

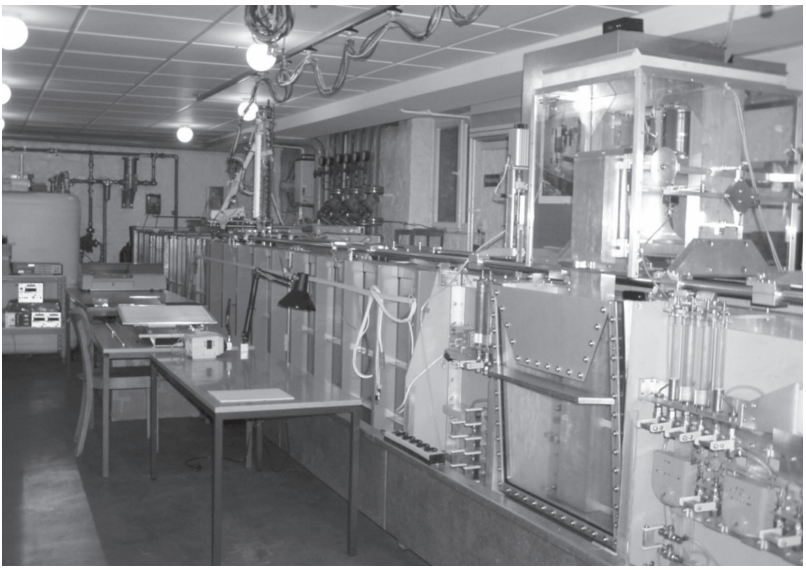

Figure 3: Photograph of the Berlin oil channel.

model similar dynamical conditions to those in the wind tunnel. In addition, an unprecedented measurement accuracy of the wall shear stress of about $\pm 0.2\%$ was achieved by the use of a differential shear stress balance [6].

Some two decades later it had become clear that a turbulent boundary layer on a surface exhibiting longitudinal ribs could develop a lower shear stress than that on a smooth surface [1, 5, 7]. When we started working in this field, we first confirmed this effect in our wind tunnel using a direct shear force measurement [8]. Subsequently we and a group from the University of Naples developed a theoretical model of the flow in the region of a riblet surface [9–11]. This model will be outlined.

The turbulent flow close to a plane smooth wall exhibits very significant instantaneous deviations from the average mean flow direction. Figure 4 shows an instantaneous streamline pattern very close to a smooth wall, as calculated by Robinson [12]. The actual size of the flow regime shown in Fig. 4 would usually be very small. For the water flow on a shark, or for the air flow on an aircraft, the actual dimensions of Fig. 4 would be in the millimetre range. In order to obtain generally applicable data, quantities are defined in dimensionless wall units. For instance, the distance y perpendicular to the wall takes the form $y^+ = y \cdot u_\tau / \nu$. This is a Reynolds number defined with the velocity $u_\tau = \sqrt{\tau_0/\rho}$, where τ_0 is the average wall shear stress. ρ and ν are density and kinematic viscosity, defined as usual. In normal circumstances, u_τ has a value equal to a few percent of the free-stream velocity. The streamwise distance x and the lateral length z are non-dimensionalized in the same way as y. In Fig. 4, instantaneous pressure levels are also given. The pressure is non-dimensionalized as $p^+ = p/\tau_0$.

The strong exchange of momentum in a turbulent boundary layer is produced by high-speed lumps of flow approaching the surface ('sweeps') and by low-speed flow moving away from the surface ('ejections') into the high-speed regions of the flow (see Fig. 4). Regions of impinging flow ('sweeps') mostly occur in regions of elevated pressure (yellow to red), whereas 'ejections', i.e. where the flow moves away from the surface, correspond mostly to regions of lower pressure

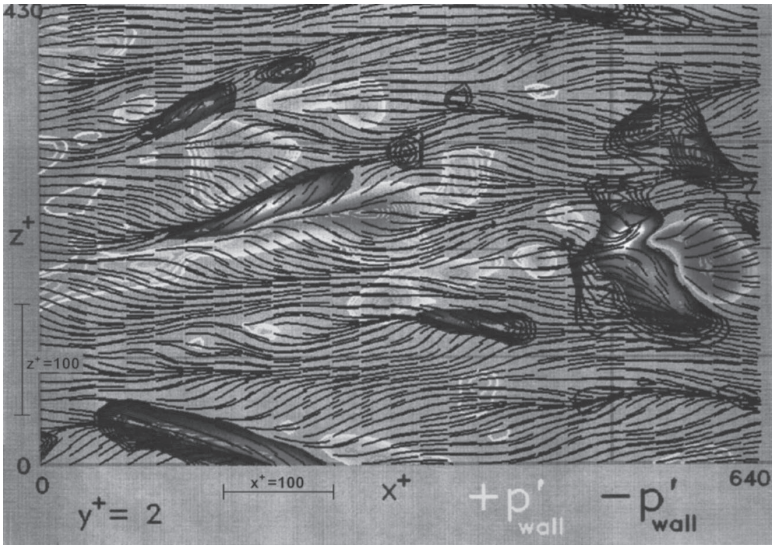

Figure 4: Instantaneous streamline pattern near a wall [12], at an elevation of $y^+ = 2$, underlaid with contours of wall pressure. Yellow to red: $p^+ = 3$ to 25; blue to white: $p^+ = -3$ to -25.

(blue to white). This exchange of fluid in a direction normal to the surface generates the enhanced shear stress of a turbulent flow because the high-speed flow is decelerated efficiently when it is swept towards the surface. By contrast, such an exchange normal to the surface does not occur in laminar flow where the streamlines are essentially parallel and the flow lacks such violent local events.

It is also obvious from Fig. 4 that local events such as 'sweeps' and 'ejections' require fluid motion in the lateral z-direction. Hampering w-velocities in the z-direction will therefore reduce momentum transfer and hence the skin friction. It is therefore plausible to suggest that a similar effect could be achieved by ribs on the surface aligned in the mean flow direction. On the other hand, it is known that surfaces exhibiting protrusions higher than about $y^+ \approx 5$ actually increase the wall shear stress [13]. However, for protrusions smaller than $y^+ \approx 3$–5, ribs or any other roughness are imbedded in the viscous sublayer. In this layer, very close to the wall, the fluid behaves like a highly viscous fluid, e.g. honey. Therefore, it is possible to use viscous theory to describe the flow around very small ribs. Under these conditions, it turns out that the ribbed surface appears as a smooth surface, but with a virtual origin (see Fig. 5).

However, the location of the origin, i.e. its elevation above the bottom of the groove depends on the flow direction. For crossflow on the ribs, the virtual origin is closer to the tips of the ribs than for longitudinal flow. The difference between these two heights we call the 'protrusion height difference', Δh. The existence of this difference has interesting consequences. Consider a fluid lump in a plane at a height y^+ above the surface; the fluid lump would experience a higher resistance if it moved laterally than if it moved in the longitudinal direction. In this way, the crossflow would be hampered by the ribs, as desired, and thus ribs would indeed reduce momentum transfer and therefore the shear stress.

Therefore, for an optimization of the shear stress reduction, we have to select a ribbed surface that exhibits a maximum difference of the virtual origins for longitudinal and crossflow. As the

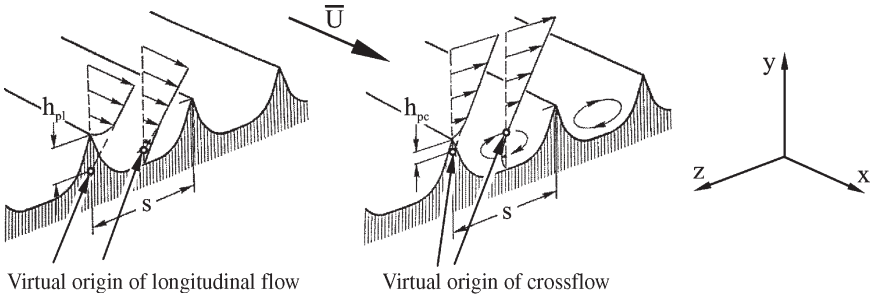

Figure 5: Longitudinal (x-direction) and crossflow (z-direction) on a ribbed surface.

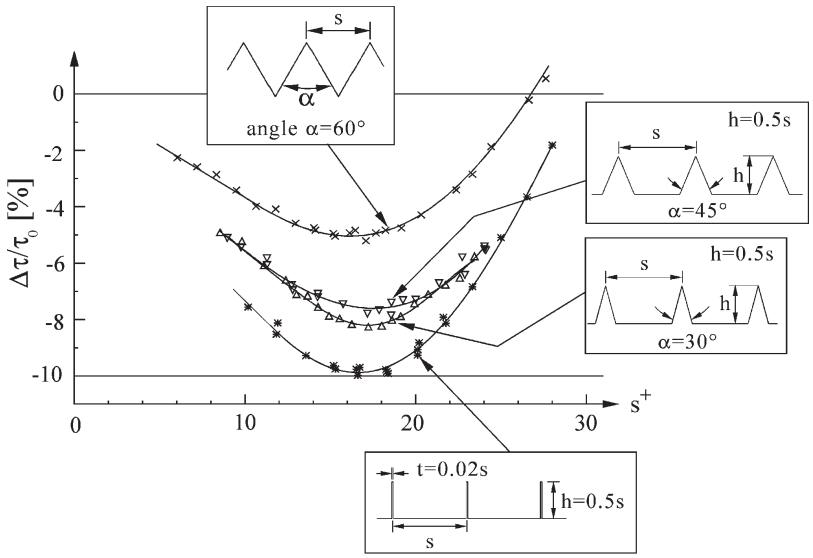

Figure 6: Drag reduction performance of various riblet geometries.

theory shows [9, 11], the maximum height difference is obtained for very thin blade-like ribs. The rib height needs to be $h \geq 0.6\,s$, where s is the lateral rib spacing. For this value of the rib height, the maximum difference of the elevation of the origins, or the protrusion height difference is $\Delta h_{\max} = 0.132\,s$. Careful experiments in our oil channel [6] with an adjustable blade rib height [14] have shown that the optimal rib height is actually slightly lower, at $h = 0.50\,s$. With this surface, a turbulent shear stress reduction of 9.9% below that of a smooth surface was achieved [14]. Figure 6 shows the data of optimal blade rib surfaces as compared to 'riblets' with triangular cross-section, which had previously been considered optimal. Clearly, it is difficult to manufacture surfaces with thin blade ribs. Therefore, we devised wedge-like ribs that still produce an impressive wall shear–stress reduction. Ribbed surfaces such as the ones shown in Fig. 6 perform well over a certain s^+ range, which corresponds to a particular velocity range. By selecting an appropriate spacing of the ribs, s, one can adjust the ribbed surface to the required flow conditions.

In Fig. 6, $\Delta\tau$ is the difference between shear stress τ on the ribbed surface and τ_0 on a smooth reference surface, i.e. $\Delta\tau = \tau - \tau_0$. Negative values of $\Delta\tau/\tau_0$ refer to drag reduction and positive values to an increase of drag.

2 Experiments with a sharkskin replica

For a long time, the aerodynamic shape and the beauty of sharks stimulated scientists to uncover their secrets of swimming effectiveness through water. There were several attempts to investigate the drag of sharks and of sharkskin. Johnson (quoted by Walsh [7]) carried out experiments using a dead brown–shark (*Carcharhinus plumbeus*) in a towing tank. Today this would be considered an effort with only a very small chance of success. It is now thought unlikely that a dead animal would show the same drag characteristics as a living one. The experiment showed a drag coefficient somewhat higher than that of a dolphin [7].

In the late fifties of the last century Petersohn [15] investigated the pressure loss in tubes lined with preserved sharkskin. The pressure data were compared with the data obtained from tubes with smooth walls: the experiments showed a higher pressure loss for the tubes with sharkskin. Unfortunately, Petersohn chose a shark species that is a slow one, the spiny dogfish (*Squalus acanthias*). Possibly, because of its availability (the spiny dogfish is present in large numbers in the waters near Scandinavia) the same species was also used by his fellow countryman Gren three decades later. In the first investigation of this kind, Gren [16] built an array of magnified plastic model scales and collected Laser Doppler data in an oil channel. He was able to change the angle of attack of the scales in two discrete steps. The scales did not have compliant anchoring. His results did not show any drag reduction of his sharkskin replica surfaces.

Independently, and at about the same time, we had tried to carry out similar wind tunnel experiments [8]. Plastic surfaces with a large number of tiny emulated shark scales were fabricated and subsequently tested using the shear stress balance [8]. The various cast plastic surfaces had scales with different angles of attack. The limitations for these latter experiments arose through: (i) the poor quality of the artificial shark scale pattern due to imperfections in the microscopic production process, (ii) the use of a surface that was again rigidly fixed and (iii) incorrectly modelled gaps between the scales, particularly at high angles of attack. The results were identical to previous findings. At high angles of attack of the scales the wall shear stress increased dramatically and only at zero angle of attack using an almost riblet-type surface could one hope for any wall shear stress reduction.

After it had been proven experimentally that riblets do indeed reduce skin friction and their shape had been optimized and a theoretical model developed, we considered the next crucial question. Are there other mechanisms at work on real sharkskins that could render an actual sharkskin superior to our fabricated surfaces? One possible mechanism might arise from the compliant anchoring of the scales that occurs on real skins allowing them to move freely.

Our oil channel [6] offered a unique tool for settling this question. By virtue of the viscosity of the oil, it was possible to emulate the microscopic features of actual sharkskin in a dimension magnified one hundred fold. Therefore, we were able to emulate (i) the detailed shape of typical shark scales, (ii) the flexible anchoring of the individual scales and (iii) a variable angle of attack of the scales with a global adjustment for all scales.

The prospect of carrying out these new experiments with scales having compliant anchoring, however, was most intriguing. Excited by high expectations, we went through the chore of building a surface with 800 individually movable scales that could also be adjusted globally to different angles of attack, as shown in Figs 7 and 8. The anchoring of the individual scales was achieved by a mechanism that is displayed in Fig. 8.

The stiffness of the suspension was adjustable through the variable clamping of the leaf springs. The spring constant could be varied over three decades from a ‘hard’ to a ‘soft’ suspension with the choice of two sets of leaf springs. In Fig. 7, the scales of a great hammerhead shark (*Sphyrna tudes*), an array of the scale replicas as well as a schematic representation of a plastic scale

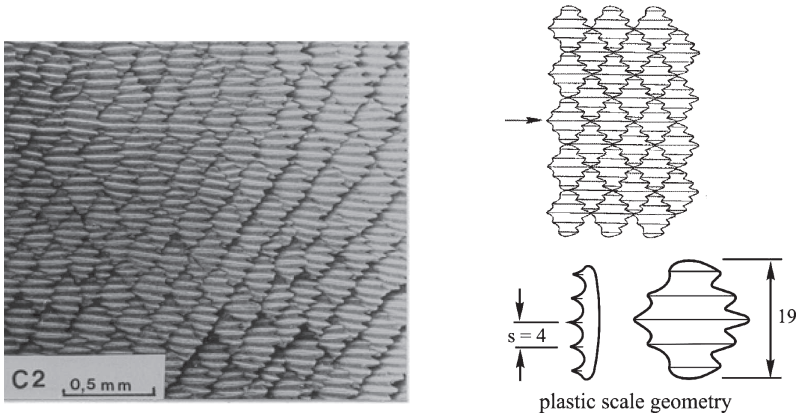

Figure 7: Hammerhead shark scales in nature and experiment, all numbers in millimetres.

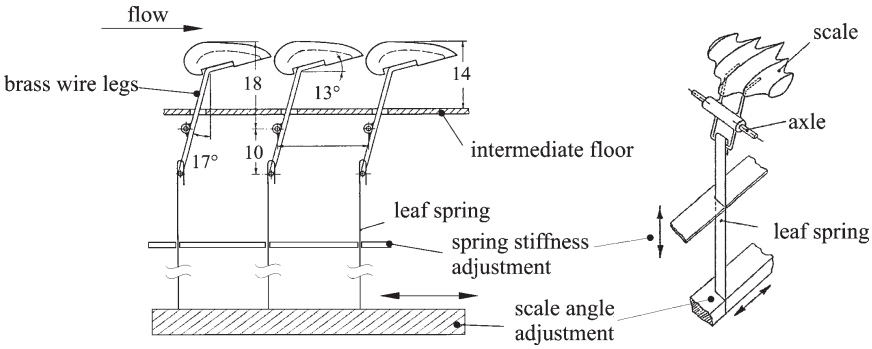

Figure 8: Schematic representation of the artificial shark scale arrangement and the suspension mechanism, all numbers in millimetres.

with five ribs can be seen. The plastic scales were designed according to our own microscope observations of hammerhead shark scales. The manufacturing process consisted first of a 600:1 hand-sculptured clay model. From that model, a negative mould was cast. With a pantograph-copy milling machine, the mould was reduced in size to a 100:1 scale. This mould was inserted into a plastic casting machine and 800 polystyrene scales were subsequently produced. In addition, tiny brass wire legs and the other parts of the suspension mechanism were manufactured using suitable tools, then soldered together and glued onto the scales. The scale array can be seen partly assembled and completely assembled in Fig. 9. Note that suspension stiffness as well as scale angle can be varied during the measurement by a remote toothed belt-drive mechanism.

Drag measurements were made with different spring stiffness with the scale both aligned and misaligned. Typical wall shear stress data measured on the artificial shark scale surface are shown in Fig. 10. For a high spring stiffness with misaligned scales the data are consistent with previous results, the misaligned scales appear to act like a rough surface and produce a large drag increase [8, 16]. An interesting situation arises when the aligned scales are anchored to the base by a soft mounting. In this case, observations in the oil-channel showed that the scales moved in a collective erratic motion, presumably driven by the locally varying instantaneous shear stresses within the

turbulent boundary layer. Nevertheless, the curve for the soft spring suspension in Fig. 10 can still be explained by quasi-static considerations. Consider the curve for the soft spring suspension in Fig. 10. For misaligned scales at low s^+, i.e. at low velocity and low shear stress, the scales remain misaligned and again behave like a stiff rough surface. As s^+ increases both the velocity and the shear stress increase. Consequently the scales are bent in the streamwise direction and thus the curve approaches that of the aligned case, resulting in a lower friction coefficient c_f consistent with the behaviour of a smooth surface.

On the other hand, if the scales are well aligned, so that the scales interlock and leave almost no gaps, we find a modest amount of shear stress reduction. This is when shark scales operate as 'riblets'. The comparatively modest performance may be due to the tiny residual gaps between the scales and other imperfections such as the lack of 'razor-sharp' rib tips. Nevertheless, this was the first time that shear stress reduction had been measured on a replica of a real sharkskin. Incidentally, for aligned scales, there was a difference between the rigid and soft suspension. In case of the soft spring suspension, the erratic motion of the scales had a minor adverse effect

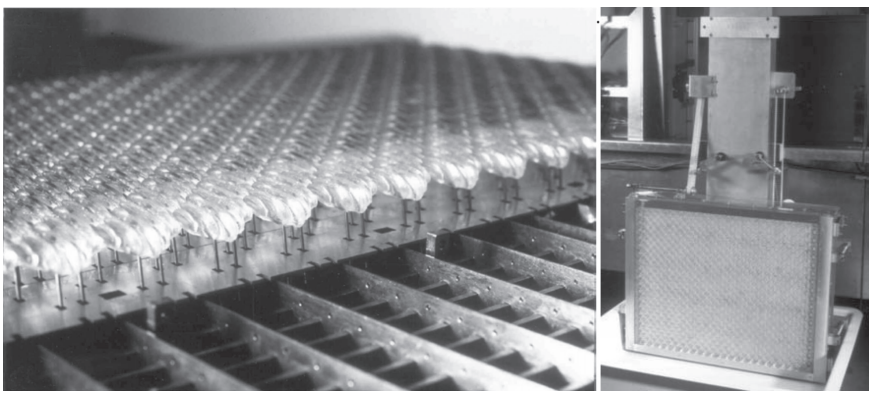

Figure 9: Sharkskin replica for oil channel tests, left: partly assembled, right: completely assembled.

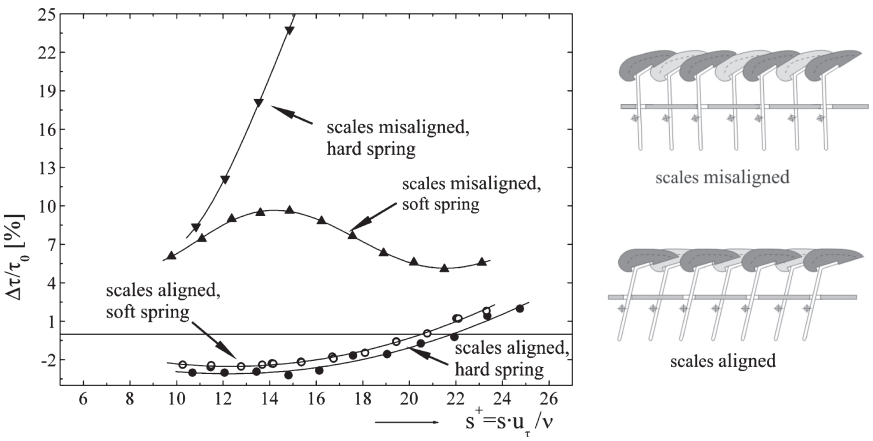

Figure 10: Typical wall shear stress data of artificial shark scales.

on drag reduction. With a rigid spring suspension the aligned scales appear stiff and the best drag reduction was obtained with $\Delta\tau/\tau_0 = -3.1\%$ [17]. This implies that the flexible mounting of the scales, allowing interaction with the turbulent flow, showed no advantage in terms of drag reduction. On the other hand, it is clear, that the shark cannot have a rigid skin structure. Otherwise, it would not be able to perform the bodily contortions required for its propulsion.

We summarize these results with the statement that, even with a detailed and compliant sharkskin replica, we did not find any striking effect, at least as far as shear stress reduction is concerned. Actually, our synthetic two-dimensional blade rib surfaces perform significantly better than our ambitious sharkskin replica. There remains, however, the possibility that actual sharkskin, say, of a shark like that shown in Fig. 1 with its very regular ribs and sharp rib tips [4], may perform better and indeed closer to our optimized synthetic two-dimensional riblets.

3 Riblets on aircrafts

Most of our data have been collected on flat surfaces with a zero pressure gradient mean flow in the streamwise direction. However, we have also carried out a few measurements on more realistic configurations. One was a test in the German–Dutch wind tunnel with a large model of the Dornier 328 aircraft (Fig. 11). Beside the expected drag reduction measured there was also a slight increase in the lift coefficient. The order of magnitude of this lift increase was 1%. The riblets also reduced the displacement thickness of the boundary layer and this effectively

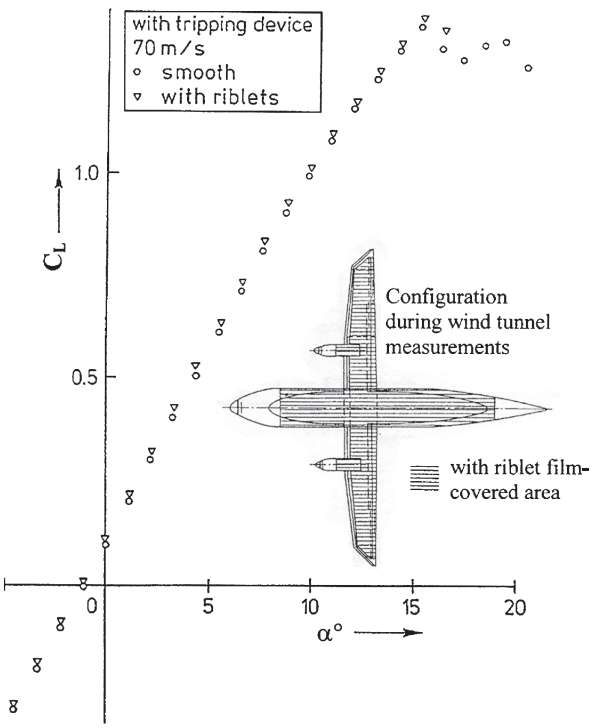

Figure 11: Measurements with a model of the Dornier 328 aircraft that was partly covered with riblet film.

increased the airfoil camber and so produced an aerofoil with higher lift properties [18]. There have been also a few tests on full-size aircraft by both Boeing and Airbus. Airbus started riblet film tests on an A320 aircraft that provided the expected results. Later, a long-range A340 airliner, partly covered (30%) with 3M riblet film was flown for several years in commercial service by Cathay Pacific Airways.

At present, artificial sharkskin, i.e. riblet film, has not been widely used on long-range commercial aircraft. The reasons why riblet surfaces are not seen on aircraft involve both rational and irrational arguments. The rational reasoning argued with technical worries, for instance, the quality of the adhesive, possible damage from UV radiation as well as a degradation in drag reduction because of fouling of the riblets from dirt. Today these arguments are no longer valid. Improved recipes for both adhesive and plastic riblet film make these arguments obsolete. The adhesive is nowadays reliable and the plastic material used for the films contains fluorine, which results in protection against UV radiation as well as acting as a dirt repellent. The perspective of having an aircraft coated with a dirt repellent film surface may offer an additional attraction as far as maintenance costs are concerned.

Besides these arguments, there is the question of application costs. At present it takes one week to coat an aircraft with riblet film, according to a certain aircraft manufacturer, and during that time the aircraft earns no money. Plausible as this sounds, it is indeed a spoof argument. Clearly, it must be possible to coat the aircraft in small regions in parallel with other mechanical or maintenance work. This is possible, because the application of the riblet film does not involve any fumes, hazardous to health, as in paint spraying.

The irrational reason consists of the prejudice of some airlines' marketing departments and aircraft manufacturers that the shimmering plastic riblet film may look unusual and therefore unappealing to customers. This could, of course, easily be changed by a clever marketing campaign.

The advantage of using riblets on aircrafts lies in both the lower fuel consumption and the resulting weight reduction. On long-range aircraft (i) the fuel costs contribute significantly to the direct operating costs and (ii) the fuel weight exceeds by far the payload.

Consider an application on an Airbus A340-300. What are the implications of riblet film to the increase of its economic performance? The contribution of the skin friction to the total drag of this aircraft is about 50%. This skin friction contribution can be reduced with our optimized riblets using trapezoidal grooves by 8.2%. Because of possible imperfection in aligning the riblets to the flow direction on the surfaces and a possible lack of extreme sharpness of the tips of the ribs it is wise to estimate the achievable drag reduction at a somewhat lower level, say with 6%. If the whole aircraft were to be covered with riblet film a total drag reduction of about 3% could be obtained. However, not the whole surface of the aircraft can be coated with riblet film for various reasons. At the leading edges of the wings and in the vicinity of the landing gear dust erosion over a long period causes damage rather like sand blasting. In addition, at the leading edges of the wings, the riblet film would interfere with the de-icing system and would also be incompatible with the laminar flow there. Locations where fuel and/or hydraulic fluid may come in contact with the plastic riblet film need also to be avoided. Obviously, neither can the windows be covered. Thus, only about 70% of the aircraft can be coated with riblet film. In addition, in some places, riblet spacing and alignment will be suboptimal.

On the other hand, some of the roughness on the aircraft surface will be covered by plastic film and will be smoothed by the film. Moreover, a reduction of the wall friction ensures a slightly thinner boundary layer that, in turn, causes a reduction of the form drag over the rear part of the fuselage. This suggests that a 2% reduction in total drag of the aircraft is probably achievable.

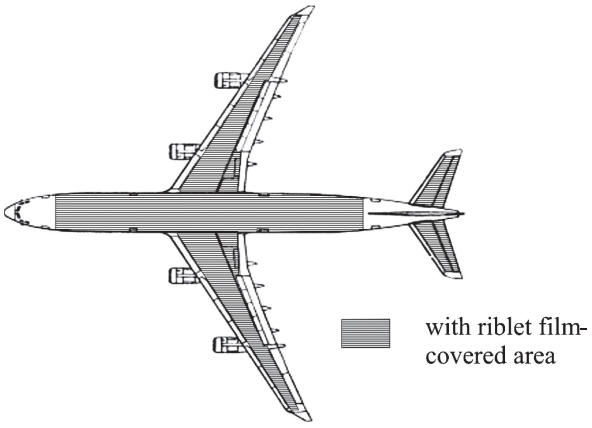

Figure 12: Long-range commercial aircraft A340-300 (Cathay Pacific) partly covered with riblet film. The film was not applied under the wing and on the lower half of the fuselage [19].

The weight of the riblet film is of the order of the weight of the paint that it replaces, i.e. 100–250 kg, depending on the percentage of the surface covered. The basic data of the A340-300 long-range aircraft (Fig. 12) are:

Empty weight	126 t
Fuel	80 t
Payload, 295 passengers	48 t
Maximum take-off weight	254 t

Currently, the share of the fuel costs is about 30% of the direct operating costs. Thus, one would save about 0.7% of the direct operating costs by a 2% reduction of the fuel consumption, attributable to a 2% total drag reduction. More importantly, about 1.6 tons of fuel can be replaced by additional payload that could be increased by 3.3%, which would be equivalent to 10 passengers. Consequently, including fuel savings the airline could be made more profitable by roughly 4%, which would add up to something of the order of a profit increase of $1 million by each aircraft per year. Incidentally, this would be roughly equivalent to what has been spent in terms of research funding on the same issue. Now one wonders whether or not this research has been too expensive.

4 Concluding remarks

The drag-reduction properties of riblet surfaces are now well understood. A viscous theory covering the flow regime where the riblets are completely covered by the viscous sublayer of the turbulent boundary layer has been established. This theory guided the choice of a riblet geometry to provide the greatest drag reduction and these forms have been confirmed by our experiments.

Although a careful investigation exploring the fluid mechanical properties of the skin of fast sharks was made, no additional insights into the secrets of the sharkskin were found. The idea that the flexibility of the skin might show an additional reduction in drag was not supported by the results of our experiments. On the other hand, one should keep in mind, that the skin

must necessarily be flexible. Otherwise, the sharks would probably have developed a more rigid structure, which would be closer to the 'technical' riblet structure.

It has been shown repeatedly that riblets can be used to reduce the fuel consumption of aircraft. Nevertheless, a standard application of this type of surface is not in sight, although all arguments (from our point of view) are in favour of using this passive drag-reducing device. When the view that the supply of fossil fuel is limited [20] coupled with the inevitable fuel price increase becomes accepted, maybe the concept of applying an artificial sharkskin to an aircraft will be reconsidered.

Acknowledgements

This paper was completed after Dr D.W. Bechert passed away in December 2004. I would like to thank Prof. M. Gaster and his wife for a careful review and valuable comments on the present paper.

References

[1] Nitschke, P., Experimentelle Untersuchung der turbulenten Strömung in glatten und längsgerillten Rohren. Max-Planck-Institut für Strömungsforschung, Göttingen, Bericht 3/1983, 1983. Trans.: Experimental investigation of the turbulent flow in smooth and longitudinally grooved tubes, NASA TM 77480, 1984.

[2] Reif, W.-E. & Dinkelacker, A., Hydrodynamics of the squamation in fast swimming sharks. *Neues Jahrbuch für Geologie und Palaeontologie, Abhandlungen*, **164**, pp. 184–187, 1982.

[3] Dinkelacker, A., Nitschke-Kowsky, P. & Reif, W.-E., On the possibility of drag reduction with the help of longitudinal ridges in the walls. *IUTAM-Symp. on Turbulence Management and Relaminarization*, Bangalore, India, 1987, eds. H.W. Liepmann & R. Narasimha, Springer-Verlag: Berlin, 1988.

[4] Reif, W.-E., Squamation and ecology of sharks, Courier Forsch.-Inst. Senckenberg, Nr. 78, Frankfurt/M., 1985.

[5] Walsh, M.J., Drag reduction of V-groove and transverse curvature riblets. *Viscous Flow Drag Reduction*, ed. G.R. Hough, Progress in Astronautics and Aeronautics, Vol. 72, AIAA: New York, pp. 168–184, 1980.

[6] Bechert, D.W., Hoppe, G., van der Hoeven, J.G.T. & Makris, R., The Berlin oil channel for drag reduction research. *Experiments in Fluids*, **12**, pp. 251–260, 1992.

[7] Walsh, M.J., Riblets. *Viscous Drag Reduction in Boundary Layers*, eds. D.M. Bushnell & J.N. Hefner, Progress in Astronautics and Aeronautics, Vol. 123, AIAA: Washington, pp. 203–262, 1990.

[8] Bechert, D.W., Hoppe, G. & Reif, W.-E., On the drag reduction of the shark skin, AIAA-Paper 85-0546, 1985.

[9] Bechert, D.W. & Bartenwerfer, M., The viscous flow on surfaces with longitudinal ribs. *Journal of Fluid Mechanics*, **206**, pp. 105–129, 1989.

[10] Bechert, D.W., Bartenwerfer, M. & Hoppe, G., Turbulent drag reduction by nonplanar surfaces—a survey on the research at TU/DLR Berlin. *IUTAM-Symp. on 'Structure of Turbulence and Drag Reduction'*, Zürich, 1989, Springer–Verlag: Berlin, 1990.

[11] Luchini, P., Manzo, F. & Pozzi, A., Resistance of a grooved surface to parallel flow and cross-flow. *Journal of Fluid Mechanics*, **228**, pp. 87–109, 1991.

[12] Robinson, S.K., The kinematics of turbulent boundary layer structure, NASA TM 103859, April 1991.

[13] Schlichting, H., *Boundary Layer Theory*, transl. J. Kestin, 7th edn, McGraw-Hill: New York, 1979.
[14] Bechert, D.W., Bruse, M., Hage, W., van der Hoeven, J.G.T. & Hoppe, G., Experiments on drag-reducing surfaces and their optimization with an adjustable geometry. *Journal of Fluid Mechanics*, **338**, pp. 59–87, 1997.
[15] Petersohn, E., Concerning an investigation of the flow in pipes, internally covered with shark skin, AE-I-444, FFA, The Aeronautical Research Institute of Sweden, 1959.
[16] Gren, P., Structured surfaces and turbulence, Licentiate Thesis, Division of Fluid Mechanics, Lulea University, Sweden, 1987.
[17] Hage, W., Zur Widerstandsverminderung von dreidimensionalen Riblet-Strukturen und anderen Oberflächen, PhD Thesis, Mensch & Buch Verlag: Berlin, 2005.
[18] Hoeven, J.G.Th. van der & Bechert, D.W., Experiments with a 1:4.2 model of a commuter aircraft with Riblets in a large wind tunnel. *Recent Developments in Turbulence Management*, ed. K.-S. Choi, Kluwer: Dordrecht, Netherlands, pp. 3–24, 1991.
[19] Jackson, P. (ed.), *Jane's: All the World's Aircraft 1997–1998*, Jane's Information Group: Coulsdon, Surrey, England, 1997.
[20] Weisz, P., Basic choices and constraints on long-term energy supplies. *Physics Today*, July 2004, American Institute of Physics, 2004.

Heat transfer enhancement techniques and their application in turbomachinery

J. von Wolfersdorf[1], B. Weigand[1] & M. Schnieder[2]
[1]*Institut für Thermodynamik der Luft- und Raumfahrt (ITLR), Universität Stuttgart, Stuttgart, Germany.*
[2]*ALSTOM Power Ltd., Baden, Switzerland.*

Abstract

Heat transfer enhancement techniques have found widespread applications in nature as well as in a lot of engineering applications. The methods can be categorized into passive and active techniques. This note focuses nearly exclusively on passive techniques, especially on heat or mass transfer enhancement using geometrical surface modifications like artificial roughness, protrusions or depressions mostly in single-phase forced convection applications. With these passive methods the flow field around the heat or mass transferring surface is modified by introducing different kinds of vortical motions, which lead to increased mixing, flow separation and reattachment. These effects drastically change the overall and local heat transfer distribution. The present paper provides an overview on the different methods used for heat transfer enhancement and shows some possible applications of the individual methods in turbomachinery design and nature. By showing examples from turbomachinery applications also the interaction of individual methods is highlighted. Here it is of particular interest that combined enhancement involving simultaneous application of several techniques might lead to an enhancement that is larger than the individual techniques operating separately.

1 Introduction

Heat or mass transfer enhancement is present in nature and in numerous engineering applications. If we look for example on the water flow through a river bed, the heat or mass transfer between the flow and the ground is intensified by the structure of the river bed, providing an artificial roughness. Therefore, one might see the 'natural' rough surface as a perfect example for a natural technique for heat and mass transfer enhancement. Heat and mass transfer enhancement is caused by flow mixing of any kind and is associated with increased turbulence in the flow. If the surface structure

WIT Transactions on State of the Art in Science and Engineering, Vol 4, © 2006 WIT Press
www.witpress.com, ISSN 1755-8336 (on-line)

is large enough and is repeated periodically, strong secondary motion might be introduced into the main flow. This leads, of course, to flow modifications and results in heat and mass transfer enhancement.

All heat transfer enhancement techniques can be subdivided into active and passive methods. Active methods are, for example, fluid vibration, injection or suction of fluid through the wall and also jet impingement to the wall. Passive methods are related to surface coatings, extended surfaces, displaced inserts, swirl flows and so on [1]. The present review paper aims to give an overview of only a small part of the different methods present to enhance heat transfer. We will mainly focus on passive methods for heat transfer enhancement using geometrical surface modifications like artificial roughness, protrusions or depressions mostly in single-phase forced convection applications. For a detailed review on other techniques, the reader is referred to the excellent book by Webb [1].

We will limit our interest in this paper mostly to the above given passive methods in single-phase flows and only on the topic of geometrical surface modifications. However, this paper cannot aim to give a complete review of all work that has been done during the last thirty to forty years on this topic. Several review papers have addressed heat transfer enhancement techniques in flows for the above specified topic and some of them are listed in [2–6]. The given review papers are not complete, but they may serve as an appropriate introduction into the interesting topic of heat transfer enhancement, especially in flows with applications to turbomachinery.

Before we go on to explain some techniques of heat transfer enhancement, it may be important first to obtain a more general view of the topic.

If one deals with the topic of heat or mass transfer enhancement, one of the questions which need to be answered first for a technical system, is the one on how "expensive" this enhancement might be; in other words, how much the friction loss of a system might increase if the heat transfer is enhanced. A first, very rough answer to this question can be given by using the Reynolds analogy between heat and momentum transfer (see for a detailed explanation Kays *et al.* [7]):

$$\mathrm{St} = \frac{\mathrm{Nu}}{\mathrm{Re}\,\mathrm{Pr}} = \frac{f}{2}, \tag{1}$$

where St is the Stanton number, Nu is the Nusselt number, Re is the Reynolds number, Pr is the Prandtl number and f is the Moody friction factor defined by

$$\mathrm{Nu} = \frac{hL}{k} = \frac{-(\partial T/\partial n)|_{\mathrm{w}}\, L}{T_{\mathrm{w}} - T_{\infty}}, \qquad \mathrm{Re} = \frac{u_{\infty} L}{\nu}, \qquad \mathrm{Pr} = \frac{\nu}{\alpha}, \tag{2}$$

$$f = \frac{|\tau_{\mathrm{w}}|}{(\rho/2)u_{\infty}^2} = \frac{|-\mu(\partial u/\partial n)|_{\mathrm{w}}}{(\rho/2)u_{\infty}^2}.$$

Here L is a reference length, k is the fluid thermal conductivity, h is the heat transfer coefficient, n indicates the normal to the surface and the indices ∞ and w denote reference states (e.g. free-stream and wall).

The Reynolds analogy given by eqn (1) is normally derived for turbulent boundary layer flows for $\mathrm{Pr} = 1$. This means that we can expect to get an appropriate answer for turbulent boundary layer type flows of gases. Equation (1) shows that there must be a strong relation in any system between heat or mass transfer and the wall friction. If we are interested in the heat transfer enhancement on a surface by the above described geometrical surface modifications, we can use eqn (1) first for a

technically smooth surface (as reference) and then for the actual surface under consideration. By doing so, one obtains for the same Reynolds number and the same working fluid

$$\frac{\mathrm{Nu}}{\mathrm{Nu}_0} = \frac{f}{f_0}. \tag{3}$$

In eqn (3), the index 0 indicates that the quantities are related to a perfectly smooth surface. Equation (3), which is a result of the Reynolds analogy, shows clearly that the ratio of a heat transfer enhancement is proportional to the ratio of the increase in friction factor. The short analysis given above also elucidates that the factor

$$E_1 = \left(\frac{\mathrm{Nu}}{\mathrm{Nu}_0}\right) \Big/ \left(\frac{f}{f_0}\right) \tag{4}$$

might be a good choice for comparing different enhancement methods [8]. There are also other methods in order to evaluate the performance of systems with heat and mass transfer enhancement features. Some of these methods have been described by Webb [9]. For example, if one is interested in the enhancement of heat transfer in an internal passage, it might be a good choice to compare several devices for the same mass flow through the passage and for the same pumping power. By doing so, one obtains a thermal performance parameter defined by

$$E_2 = \left(\frac{\mathrm{Nu}}{\mathrm{Nu}_0}\right) \Big/ \left(\frac{f}{f_0}\right)^{1/3}. \tag{5}$$

This parameter has been very popular for evaluating different heat transfer enhancement schemes for compact heat exchanger. In the following sections, we will actually use both criteria in order to evaluate different enhancement techniques.

2 Heat transfer enhancement techniques

This section is devoted to different heat and mass transfer enhancement methods based on surface geometrical modifications. Each technique will be explained and their potential for heat and mass transfer enhancement will be discussed.

Section 2.1 deals with surface roughness. This is a typical (mostly) stochastic roughness as appears in many natural and technical processes. Section 2.3 of this chapter is devoted to ribs and turbulators. These are features which are normally larger than the thickness of the boundary layer and which produce strong secondary motions within the flow field. Section 2.2 deals with small scale features of this kind, which have a height of the order of the boundary layer thickness or smaller, but consist of regular manufactured rib type structures. In addition, the features discussed in Section 2.2 do not produce strong secondary motion because of their placement and design.

There is of course no clear separation between the features discussed in Sections 2.1 and 2.2, but we decided to introduce this distinct separation between the (normally) stochastic roughness in Section 2.1 and the small features in Section 2.2 in order to make things clearer.

2.1 Surface roughness

Rough surfaces are found in many configurations in nature and design. Turbulent flows over rough surfaces occur in a multitude of situations in engineering applications and in natural environment. Examples range from the flow over plant canopies [10], ship surfaces under the influence of

biofouling [11], boundary layers over desert sand dunes or sediments [12, 13] or water flow over mussel beds and coral reefs [14, 15]. In engineering, rough surfaces are used to enhance heat transfer using, for example, randomly arranged sand grains or regular two- or three-dimensional roughness elements. The importance in heat and mass transfer enhancement as well as surface friction has led to numerous investigations. Early work by Nikuradse [16], Schlichting [17] and Moody [18] provided fundamental data for the analysis of turbulent flows and a framework for the interpretation of roughness effects on flow and heat transfer.

Nikuradse [16] measured pressure loss and velocity profiles in pipes roughened with nearly uniform sand grains of different sizes with the characteristic dimension denoted as k_s. Based on these measurements, Schlichting [17] determined for other roughness structures with roughness height k an equivalent sand-grain roughness parameter, defined as the sand grain size in Nikuradse's experiments that gives the same friction loss at the same Reynolds number. The ratio k_s/k depends on the geometry and surface density of the roughness. Schlichting [19] correlated this ratio in dependence of the solidity Λ, which is the total projected frontal roughness area per unit wall-projected area. With this, the effect of roughness on the flow field can be related to the velocity profile over the surface and compared with the smooth wall situation. The mean velocity profile in the inner region of a turbulent boundary layer at a smooth wall is described by the classical log law [17]:

$$U^+ = \frac{1}{\kappa}\ln y^+ + C, \tag{6}$$

with the quantities

$$y^+ = \frac{yu_\tau}{\nu}, \qquad U^+ = \frac{u}{u_\tau}, \qquad u_\tau = \sqrt{|\tau_w|/\rho}. \tag{7}$$

Here, y^+ is a dimensionless wall distance, measured from the wall into the boundary layer, u_τ is the shear–stress velocity, κ is the von Karman constant and C is an additional constant.

For a rough wall, Clauser [20] showed that the primary effect of the roughness causes a downward shift ΔU^+ in the log law, obtaining a generalized description for smooth and rough walls (see Fig. 1):

$$U^+ = \frac{1}{\kappa}\ln y^+ + C - \Delta U^+ \tag{8}$$

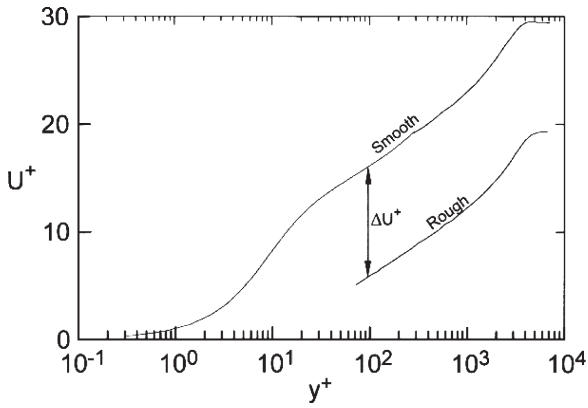

Figure 1: Typical mean velocity distributions, normalized using wall variables, over smooth and rough walls (from [21]).

The roughness function ΔU^+ depends on the roughness Reynolds number k_s^+ defined by:

$$k_s^+ = \frac{k_s u_\tau}{\nu} \tag{9}$$

Schlichting [17] characterized the surface roughness using this parameter. For $k_s^+ < 5$ the surface is considered to be hydraulically smooth and frictional losses depend only on the Reynolds number. In this case the roughness elements are embedded in the so-called laminar sub-layer and momentum is transferred solely by shear stresses. For $k_s^+ > 70$ the flow is considered fully rough and frictional losses depend only on the dimensionless roughness height. Momentum is in this case is transferred to the wall by pressure forces. For $5 < k_s^+ < 70$ the transitional region is present where both, roughness height and Reynolds number, influence the frictional behaviour.

For so-called 'k-type' roughness (e.g. regular transverse ribs, see Section 2.2), often the roughness height k is chosen as the characteristic length scale. A Reynolds number based on the roughness height is then given as:

$$\mathrm{Re}_k = k^+ = \frac{k u_\tau}{\nu}. \tag{10}$$

Both eqns (9) and (10) are related using the ratio k_s/k. The logarithmic behaviour of the velocity profile is similar for flows over rough surfaces in nature. An excellent review was given by Raupach *et al.* [10]. They compared data from artificial rough surfaces from laboratory experiments with atmospheric data from several vegetation surfaces. Although the k^+ values for the vegetated surfaces were up to two orders of magnitude higher than the laboratory data, the logarithmic behaviour was almost the same in the fully rough regime.

The roughness function is not uniquely determined by the roughness Reynolds number [21] and therefore not universal for different roughness types. Important influences come from the roughness density, roughness shape and regularity of the roughness elements. Therefore there are still difficulties in identifying a length scale that characterizes a particular roughness geometry [22]. As already noted by Schlichting [17], there are differences in the friction loss between the data from uniform diameter sand-grains used by Nikuradse [16] and data from irregular or sparse roughness. The differences are most pronounced in the transitional region as shown in Fig. 2 [23].

Also, the critical roughness Reynolds numbers, below which roughness does not affect the flow or at which the flow becomes fully rough, are still subject of investigations with respect to very high Reynolds numbers [24] or atmospheric boundary layers [25] in view of the variety of irregular surface roughness mostly found in nature. The behaviour of transitionally rough surfaces has been reviewed by Bandyopadhyay [26] and more recently by Jimenez [27]. He noted, that much of the investigations before 1990 concerned the universal aspects of flows over rough walls. More recently the research focuses on the different types of roughness. Van Rij *et al.* [28] investigated irregular surface roughness and correlated the data using a roughness parameter which includes a roughness density parameter as well as a roughness shape parameter introduced by Sigal and Danberg [29]. Since the roughness height varies in this case over the investigated surface, an average value needs to be determined. This is accomplished by using a high-resolution optical surface profilometer.

A main impetus for this research comes from turbomachinery. Modern gas turbines operate in harsh environments with high temperatures and flows with particles from the combustion products for long periods between inspections or maintenance. Because of this, the turbine components experience significant degradation over time due to particle deposition, erosion or high temperature corrosion leading to a very non-regular roughness structure on the surface [30]. Surface roughness

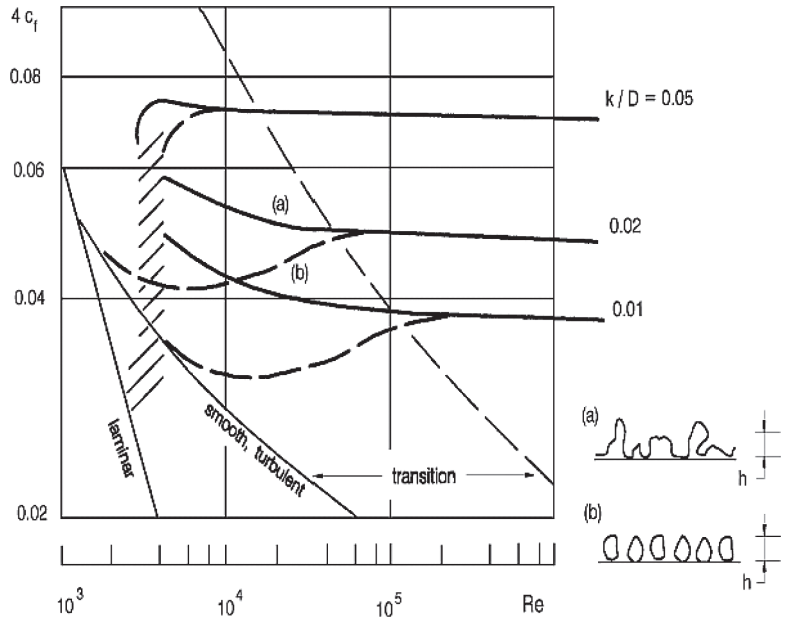

Figure 2: Influence of different roughness types on the friction factor behaviour (from [23]).

on blades and vanes influence gas turbine performance due to the elevated levels of surface friction and the higher heat loads due to the heat transfer enhancement. Hence, modelling approaches are still limited due to the irregularity of the roughness structure. A good understanding regarding profile losses and heat transfer enhancement for these 'natural' surfaces is therefore required [31, 32].

Let us now focus on some observations from rough surfaces in nature with respect to mass (heat) transfer. A prominent example is the flow over coral reefs. An important challenge which ecologists face today is to explain, how these ecosystems maintain a high productivity under relatively low concentrations of nutrients required for the coral growth. This point is termed the Darwin paradox [33]. A large number of investigations using wind tunnel tests [34], water tests with coral reef flat assembles [35], recirculating flow chambers using single coral heads [36] and coral skeletons in flow tanks at different flow speeds [37] have been performed. The boundary layer characteristics were found to follow the log law relationship [38]. Engineering correlations as developed by Dipprey and Sabersky [39] were used to compare the determined mass transfer although the Schmidt number (Sc) was generally larger than in the engineering studies. Very high mass transfer rates (up to six times the predicted values from the engineering correlations) were found [15, 33] and possibly related to the very high surface area and the fractal nature of the surface or the interaction of the biomass element motion with the flow. Difficulties exist, of course, in defining the appropriate roughness length scale in these cases of large variations in roughness scale. Each chosen length scale will give another friction prediction for a given flow situation [35]. Using measured friction losses and there from defined roughness scales (as the sand grain roughness) makes a better match to the engineering data [40]. Mass transfer relationships for several corals were developed by Patterson *et al.* [36]. The coral heads used in this study where hemispherical to almost spherical and compared to engineering correlations for flow around cylinders or spheres. In most cases, the mass transfer between the organism and the environment increased with flow rate.

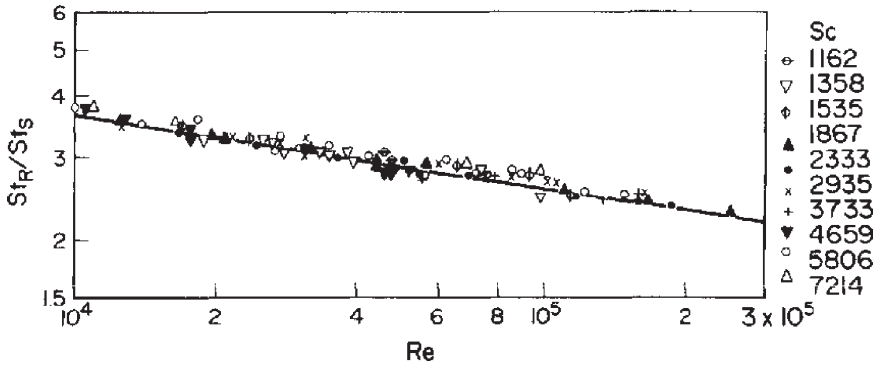

Figure 3: Mass transfer enhancement for small ribs in a channel compared to a smooth channel (R, ribbed channel; S, smooth channel) at different Schmidt numbers (Sc) for $e/D = 0.0364$ (from [51]).

On the other hand, when the flow was increased to values in the upper range of those encountered in nature, the mass transfer enhancement effect decreased. This is similar to what is given below for a constant roughness size with increasing Reynolds number (see Fig. 3). It seems therefore that nature adapts the element size to the respective flow conditions for maximum transfer capability. Patterson *et al.* [36] noted that the organisms do generally better than predicted by available theory. Possible explanations are related to the role played by small parts (e.g. cilia) disrupting the laminar sub-layer, the skeletal morphology or the concentration gradients developing due to the interaction of the biomass with the overlying seawater. Gardella and Edmunds [37] suggested that the boundary layers around small corals are heavily influenced by larger upstream roughness elements. These larger elements can introduce vortical motion and mixing processes near the surface and thereby enhancing mass transfer. Flow separation and reattachment is observed in most aquatic boundary layers and sudden changes in boundary roughness, from smooth to rough or vice versa, are very common in marine environments [41]. Other effects could be related to biological processes such as respiration or photosynthesis [38] or the overall survival capability of the animal. Commito and Rusignuolo [14] noted that the surface roughness of mussels influence the rate at which the mussels are eaten by predators or dislodged by water currents.

So far our understanding of the heat (and mass) transfer enhancement processes on natural, irregular surfaces is still limited. The advances in two- and three-dimensional optical surface measurement equipment and the capability of producing plastic roughness models using fast prototyping techniques for irregular surfaces [28, 31] will provide a deeper understanding in this context. Together with the application of full surface temperature, pressure or concentration measurement techniques (e.g. [109]) a better knowledge of roughness effects on heat (mass) transfer enhancement in nature and engineering may be obtained. Many studies applying these techniques have been used to measure detailed information for e.g. turbulated cooling channels in gas turbine components. Numerical simulations combined with such experiments will help in this context. Several modelling approaches for rough surfaces were reviewed by Patel [42] and their limitations have also been discussed. More recently Large Eddy Simulations (LES) [43] and Detached Eddy Simulations (DES) [44] have been applied to resolve the actual irregular roughness geometry in three-dimensional computations.

2.2 Small scale regular repeated roughness

Regular repeated roughness like ribs is widely used for heat transfer enhancement in the internal cooling circuits of gas turbine blades and vanes, for combustor liner cooling in heat exchangers and for fuel pins in gas-cooled nuclear reactor parts among others. Even for regular structures there are many possible shapes and arrangements such as regularly spaced ribs of any shapes located perpendicular to the main flow or provided with an angle to the flow. These are often referred as two-dimensional roughness. A uniform or random distribution of protrusions of any shape on a surface is termed three-dimensional roughness [45, 46]. The height of the roughness elements is denoted by e, to distinguish this machined or casted roughness from naturally occurring structures or the sand-grains discussed before. The non-dimensional roughness parameter e^+ is then used to analyse, characterize and correlate the data:

$$e^+ = \frac{eu_\tau}{\nu}. \tag{11}$$

Earlier studies from the heat exchanger and nuclear reactor area have mainly focused on small size roughness (roughness height e less than 5% of the channel height) and high Reynolds numbers. The rib height-to-channel height ratio and the pitch distance between the ribs were found to be important parameters.

Sheriff and Gumley [47] performed experiments in annuli with wires wrapped around the inner tube for different wire sizes at a pitch-to-wire diameter ratio of 10. They showed that the heat transfer enhancement over a smooth surface reached values up to 2.3 for measurements in air and could be approximately correlated using e^+. The smaller roughness did not correlate well at low e^+ and the heat transfer enhancement was not constant for the higher values of e^+. Their results further showed that the heat transfer enhancement factor increases with increasing e^+ but levels off for e^+ larger than 100. An optimum heat transfer surface having good heat transfer enhancement at moderate friction increase should therefore be considered having $e^+ < 100$. Sheriff and Gumley [47] defined their optimum heat transfer surface to have a value of $e^+ \sim 35$.

Two-dimensional roughness elements were studied by Nunner [48] in tubes. Heat transfer enhancement was found to be always lower than friction loss increase. For frictional losses larger than four times the loss in a smooth pipe, the heat transfer enhancement stayed constant. Rough tubes with close-packed, granular type, roughness elements were studied by Dipprey and Sabersky [39] using water as the working fluid to cover a wider range of Prandtl numbers. Heat transfer enhancement due to roughness as high as 270% was obtained. At the higher Prandtl numbers at least one roughness type gave a larger heat transfer increase than the associated friction loss increase. It was noted that this favourable condition occurred in the transitional rough regime rather than in the fully rough regime. Kader and Yaglom [49] applied similarity between heat and mass transfer to analyse rough walls from heat and mass transfer experiments for large Prandtl and/or Schmidt numbers (see e.g. [110]).

The experiments from Dawson and Trass [50] using V-shaped grooves as roughness elements at very large Schmidt (Prandtl) numbers reached enhancement factors between three and four for dimensionless roughness heights of about $e^+ \sim 10$. Here it should be taken into consideration that the thermal or concentration boundary layer is very thin for large Prandtl (or Schmidt) numbers. This means that the main variation in concentration or temperature takes place in a very thin layer near the wall. Relating these experiments to the equivalent sand grain roughness, Kader and Yaglom [49] showed that this maximum mass transfer enhancement occurs at $k_s^+ \sim 25$.

Mass (heat) transfer enhancement with small square ribs in a tube were investigated by Berger and Hau [51]. The rib parameter e/D (rib height to tube diameter ratio) was kept constant at

0.0364 and the Reynolds and Schmidt numbers were varied over a large range. It was shown, that the heat transfer enhancement (given as Stanton number ratio between rough and smooth tube) decreases with increasing Reynolds number for the constant roughness height considered (Fig. 3) for a large range of Schmidt numbers. Therefore the roughness height should be adapted to the actual Reynolds number (flow velocity) for efficient heat transfer enhancement.

Stochastic roughness structures are not very often used in engineering for heat transfer enhancement. More often, machined ribs of regular patterns are used. If the rib heights are small, the roughness Reynolds numbers are in the range of the transitional and fully rough regimes and can be well related to roughness structures as the sand grain roughness. One of the most general correlations for such transverse rib-repeated roughness were presented by Webb *et al.* [52] for e/D between 1% and 4%, p/e between 10 and 40 and Prandtl numbers between 0.71 and 37.6. The pitch to rib height ratio p/e was related to different flow patterns as given in Fig. 4.

For small spacings ($p/e < 5$) a closed recirculation region was found between the ribs. For larger spacings the separated flow reattaches between the ribs and a new boundary layer develops. In front of the next rib another recirculation region appears. The reattachment point is approximately 6–8 rib heights downstream from the separation point.

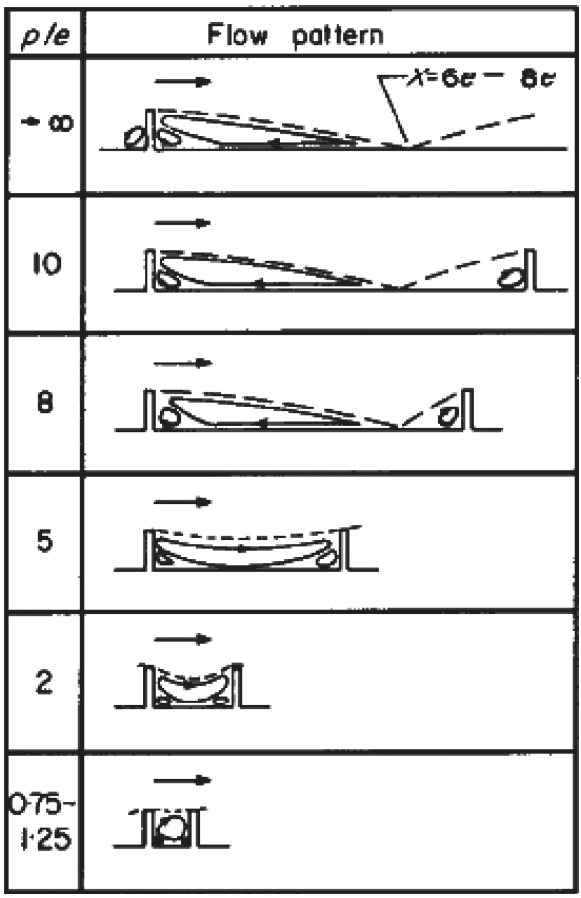

Figure 4: Flow pattern as a function of pitch to rib height ratio p/e (from [52]).

2.3 Ribs and turbulators

The above given work of Webb *et al.* [52] was extended by Han *et al.* [53] for larger rib heights in view of gas turbine internal cooling. The cooling channels in gas turbines used in aircraft engines usually have small dimensions, leading to relatively low Reynolds numbers in the turbulent flow regime (Reynolds numbers below 50,000). Achieving large heat transfer enhancement for these conditions requires larger rib heights. Moreover, for manufacturing reasons the physical size of the rib elements has to have a minimum value which leads to large relative rib heights (up to 25%). With the importance in gas turbine component cooling, numerous investigations have been performed in this context.

The ribs are usually placed in a repeated manner to disturb the boundary layer periodically leading to high turbulence levels and good mixing in the coolant core flow. It has been found that the flow achieves a periodic 'fully developed' state after about five ribs. Because of their importance, a large body of work has been done, and is still continuing to be done, to understand the effects of different rib turbulators on pressure drop and on heat transfer in, for example, square or rectangular channels.

This work was summarized and reviewed by Han and Dutta [54], Taslim [55], Ligrani *et al.* [8] and in a book by Han *et al.* [56]. In the process, the influence of rib spacing, rib angle and rib height has also been investigated. Angled ribs introduce swirling motion in the flow and therefore increase mixing as well as local heat transfer. The ribs can be continuous or broken or have V-shaped form [57, 58]. By this, the number of vortices introduced in the core flow can be varied. The resulting secondary flows can be adopted using different rib arrangements on opposite walls of the cooling channel.

Figure 5 shows some experimental results for the local heat transfer in a rectangular duct with V-shaped ribs. On the left, the secondary flow field and the associated effect on the heat transfer is depicted for ribs pointing downstream in flow direction, whereas the figure on the right shows the situation for a V-shaped ribs pointing upstream. From the two figures it can be seen that the heat transfer can be locally adapted by selecting appropriate turbulators. For example, for the arrangement shown on the left side in Fig. 5, the secondary motion takes fluid from the centre region in the passage upwards and transports this fluid towards the sidewalls. Near the sidewalls a downwash of the fluid can be observed, resulting in high heat transfer at this location.

The effective generation of strong secondary flows with these ribs has led to a variety of investigations in view of optional arrangements. V-shaped ribs combined with V-shaped grooves in between were investigated by Zhang *et al.* [60]. Wright *et al.* [61] measured average heat transfer and friction losses for V- and W-shaped ribs. The latter are a combination of smaller scale V-shaped ribs. The effect of separating the ribs and staggering them on one wall (so-called discrete arrangements) was shown to increase heat transfer further by reducing the frictional losses slightly compared to full ribs [62].

Compared to the heat transfer requirements for aero-engine blades, the cooling schemes of blades for large industrial gas turbines differ in some aspects [5]. An important difference is that blades for heavy-duty gas turbines are subjected to higher Reynolds numbers in the internal cooling passages mainly due to their much larger dimensions. The larger size of the internal cooling passages gives much more freedom in designing the shape of cooling and heat transfer enhancement features like ribs inside the blades. Thus, rib geometries can be adapted to the actual cooling channel form, which is usually not square or rectangular. Typical examples are the cooling channels near the leading and trailing edge of the blade or channels of aerodynamically optimized blades for later stages (see Fig. 6, [63]). All these ducts might be approximated by triangular channels.

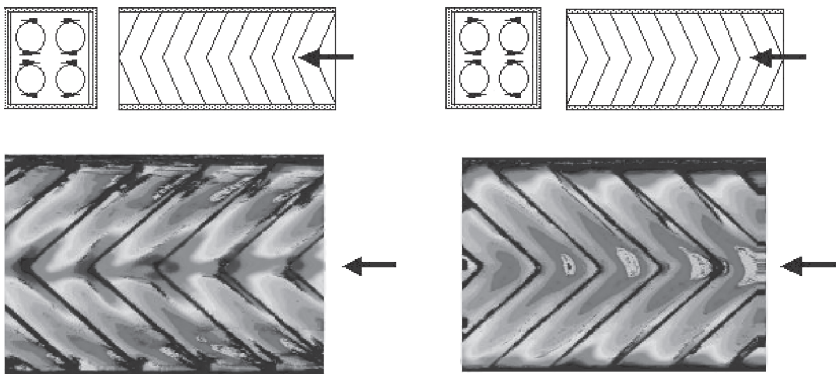

Figure 5: Heat transfer distribution in a rectangular channel with varying orientation of V-shaped ribs (adapted from [59]).

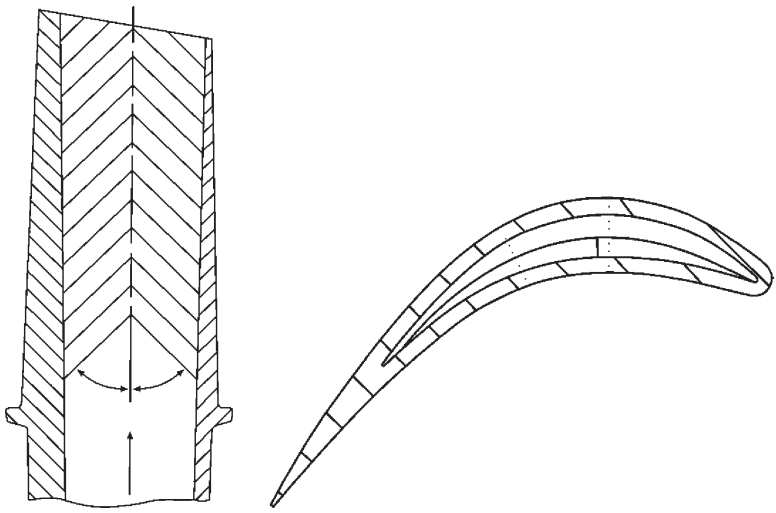

Figure 6: Cooling scheme for a rotating blade at later stages using size-adapted V-shaped ribs (from [63]).

Within these channels three-dimensional shaped turbulators can be manufactured for industrial gas turbine blades. By this, the local heat transfer can be influenced drastically. Figure 6 shows such an arrangement. The rib height is gradually decreased with decreasing channel height. Hall *et al.* [63] used the criterion, that the local height of the rib h divided by the local channel height H is constant. Applying this criterion, the local friction in the channel between the core region and the apex area is equalized. This promotes the secondary flow to exchange air between the core area and the apex area, leading to higher heat transfer coefficients in the edges where the heat load from the hot gas side is highest. Three-dimensional shaped turbulators can also be used for effectively cooling the leading edge of a gas turbine blade. Figure 7 shows an example of such an application [64]. The three-dimensional ribs are additionally angled with respect to the main flow direction (see the picture on the left in Fig. 7) and can have different overlapping arrangements in the corner area. In addition, the rib spacing can vary, to adapt the heat transfer enhancement

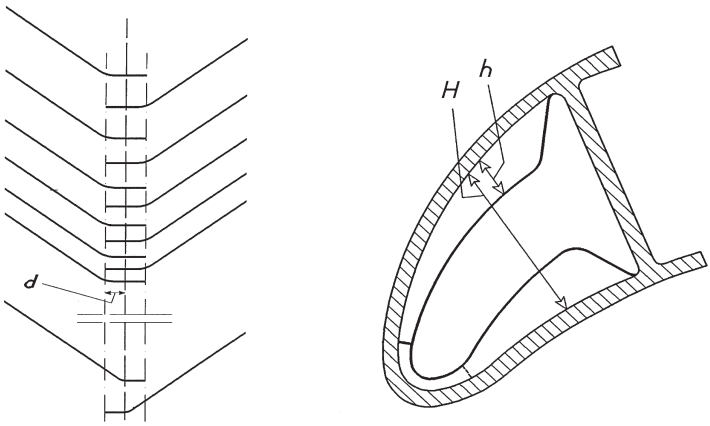

Figure 7: Three-dimensional turbulators for a leading edge cooling channel of an industrial gas turbine blade (from [64]).

to the local cooling requirements. With this, local heat transfer distributions can be tailored along the channel circumference to achieve small temperature differences and, hence, small thermal stresses within the blade. Some examples for a triangular channel, typically for the leading edge cooling channel of a blade, are shown in Fig. 8.

From Fig. 8 it is obvious that the local extension of the rib in the leading edge area will affect the heat transfer in this area substantially. The upper picture in Fig. 8 shows overlapping ribs in the leading edge region at an angle of 45° to the main flow direction whereas the lower picture in Fig. 8 is for a configuration with every second rib removed and arranged at an angle of 90° to the main flow direction.

Recent applications of V-shaped ribs are also found in microfluidic systems, which are widely used in biology and biotechnology [65, 66]. Due to the small channel sizes, the flow in these systems is usually laminar with Reynolds numbers well below 100. Therefore, mixing of different streams, e.g. for chemical analysis, is limited. V-shaped ribs with offset apex angles can provide efficient mixing in these cases. The apex location changes in flow direction after several rib modules leading to a so-called staggered herringbone mixer. Thereby the size of the counter-rotating vortices as given in Fig. 5 is unequal and changes in streamwise direction, which is the basis for the good mixing behaviour. Other geometries, which introduce such longitudinal vortices are known in the context of boundary layer control and heat transfer enhancement and will be discussed next.

2.4 Longitudinal vortex generators

Several kinds of vortex generators introducing longitudinal vortices in the near-wall region have been considered for boundary layer separation control [67] and associated lift enhancement or noise reduction [68]. The size and shape of the vortex generators can be very varied. In nature, smaller size vortex generating fins are known on the back of several types of fish and act possibly as boundary layer control devices [69]. Larger finlike structures were recently related to thermoregulation of animals. Meagher *et al.* [70] measured the temperature field on a bottlenose dolphin dorsal fin. These fins contain many blood vessels to either conserve or dissipate body heat. With high surface heat transfer due to separating vortices, these fins might be effectively used for fast control of the body temperature, since longitudinal vortices are more efficient than

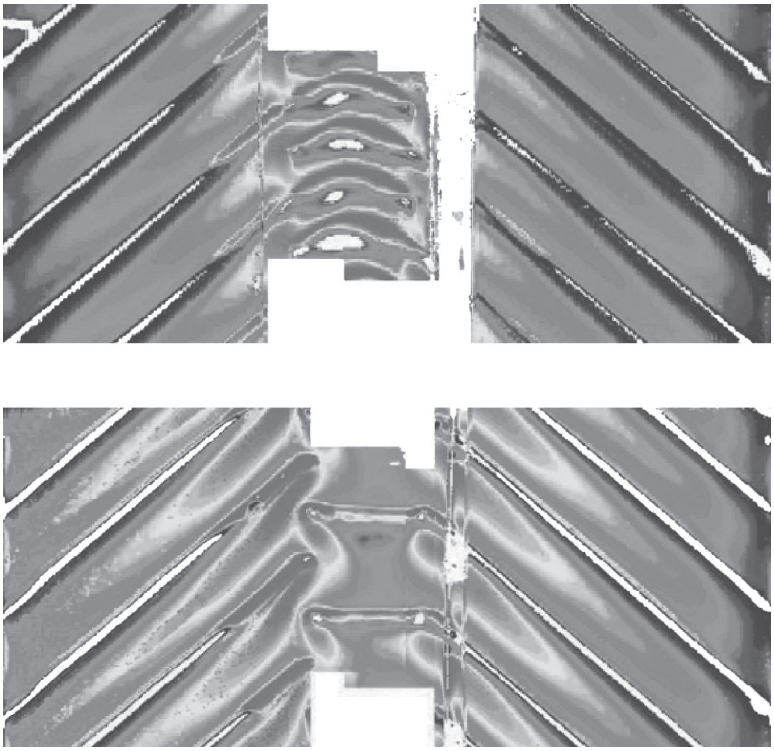

Figure 8: Local adaptation of heat transfer distribution using different rib configurations in the leading edge region (from [107]).

transverse vortices for heat transfer enhancement. The use of longitudinal vortex generators for heat transfer enhancement is mainly considered in the area of heat exchangers. Good reviews on these developments can be found in [71–73]. Several geometries, which can easily been manufactured for plate heat exchanger applications were considered and are shown in Fig. 9. They are called wing or winglet vortex generators.

In a pairwise arrangement, the winglets introduce neighbouring streamwise vortices, enhancing the near-wall momentum exchange and heat transfer. Similar to the above-described V-shaped ribs, the vortex pair can be arranged to form a downwash motion or an upwash motion. This is shown in Fig. 10 using a pair of delta-winglet vortex generators. A common inflow vortex pair is generated using the configuration as given in the picture on the left in Fig. 10. The induced inflow thins the thermal boundary layer and strongly enhances heat transfer.

The arrangement given in the picture on the right in Fig. 10 generates a common outflow vortex pair with associated lower heat transfer. Since the projected area perpendicular to the flow for these devices are generally smaller than for ribs, cylinders, or cubes, heat transfer enhancement can be found at relatively moderate pressure loss increase. The induced vortices are very persistent and can survive more than 100 vortex generator heights downstream depending on the individual geometrical and flow parameters and can introduce transverse velocities in the order of the streamwise velocity [71].

Arrangements of several winglet pairs have been used in rectangular channels [73] or have been combined with circular or oval tubes in plate and tube heat exchangers [74, 75], which themselves

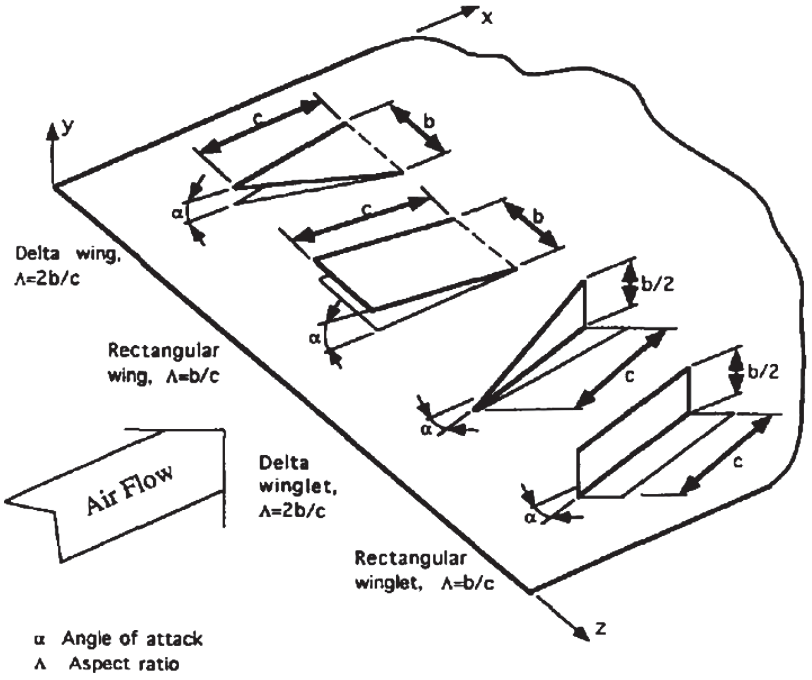

Figure 9: Vortex generators and associated definitions (from [71]).

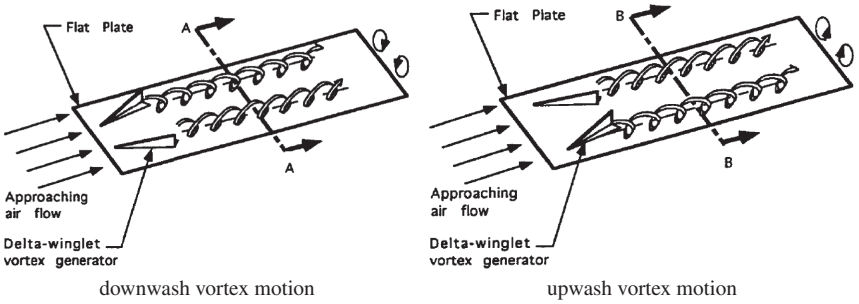

downwash vortex motion upwash vortex motion

Figure 10: Schematic representation of induced vortex pairs; left: common inflow; right: common outflow (from [71]).

generate longitudinal vortices around the tubes, the so-called horseshoe vortex. It was noted by Fiebig [72] that the vortex generator form, height, length, angle of attack and spacing have not yet varied appreciably, which points towards optimum values for heat transfer enhancement at small pressure losses. Furthermore, the efficiency of these devices at high Reynolds numbers is not known well. The Reynolds numbers in plate heat exchangers are usually between 3,000 and 30,000.

For other applications, e.g. in gas turbine cooling, the Reynolds numbers are in many cases much larger. Besides this, the vortex generator elements need to be cast for gas turbine applications, leading to the consideration of delta-shaped solid vortex generators. A schematic representation of such a vortex generator and the expected flow field is shown on the left in Fig. 11.

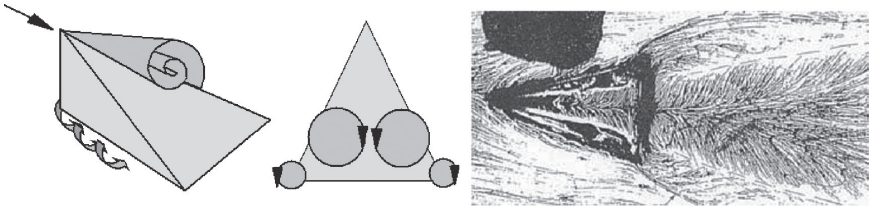

Figure 11: Schematic representation of flow field around a delta-shaped solid vortex generator (left) and near-wall streamlines from an oil visualization study (right).

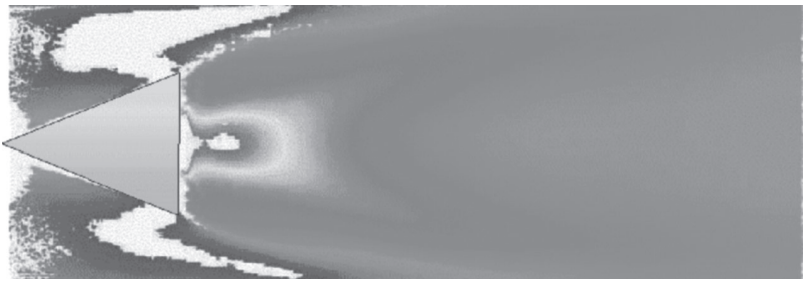

Figure 12: Heat transfer distribution behind a single delta-shaped solid vortex generator.

Similar to the delta winglets, a pair of counter-rotating vortices develops above the vortex generator. Additionally, a kind of horseshoe vortex is generated on the base of the vortex generator, which has a lower vortex strength. The effect of these vortices on the near-wall flow is visualized on the right in Fig. 11 using an oil streak visualization technique. The effect of both vortex pairs can be well observed. The vortex strength of the main pair directly behind the vortex generator is very large and the transverse velocities are larger than the streamwise velocity there. This can be deduced from the nearly 'vertical' oil-streak patterns in this region. This is also the region of highest heat transfer, as shown in Fig. 12. Afterwards, the vortex strength decays and the vortex pair diverges, as can be well seen in the heat transfer distribution. Flow velocity measurements of the secondary flow field as obtained by Particle Image Velocimetry (PIV) are given in Fig. 13 and can be compared to the schematic flow field given in Fig. 11.

Arranging the vortex generators in a repeated manner will change the situation drastically. This is shown in the flow visualization given in Fig. 14 for a staggered arrangement. Vortices from the upstream rows interact with the downstream generated vortices. For close arrangements, as given in Fig. 14, the upstream vortex pairs will be pushed together by the downstream configurations, thereby avoiding the convergence of the vortices.

A heat transfer investigation of such arrangements in a square channel was presented by Han *et al.* [76]. Vortex generators were placed on two opposite walls of the test channel. The measurements revealed the good heat transfer enhancement capability of the vortex generators and also investigated the associated pressure losses. Forward and backward directed vortex generators were studied. The backward direction refers to the flow direction as given in Fig. 11. For the forward situation, the flow direction is opposite to this with respect to the vortex generator. It was found that the backward direction enhances heat transfer more than the forward direction. An aligned arrangement of vortex generators in subsequent rows gives higher heat transfer than an offset or

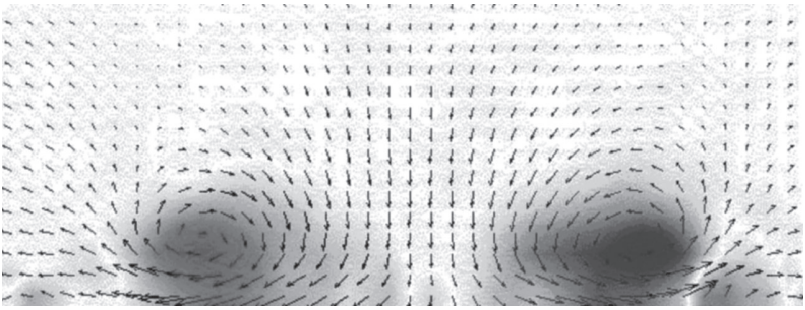

Figure 13: Secondary flow behind a delta-shaped vortex generator as measured by PIV.

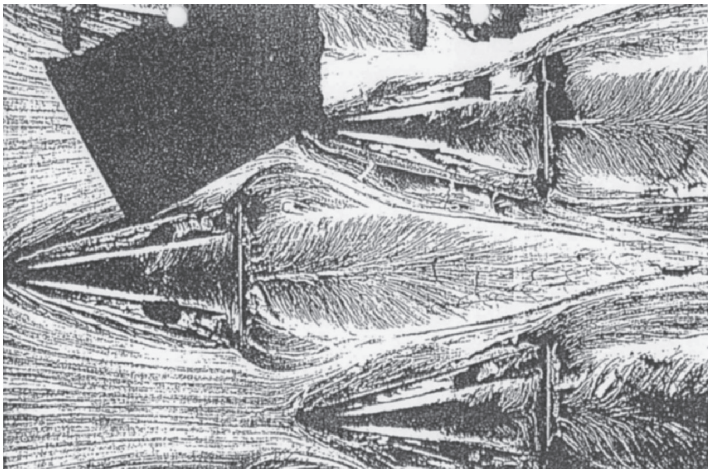

Figure 14: Oil flow visualization for a staggered array of delta-shaped solid vortex generators.

staggered arrangement. This suggests that, due to the alignment of the elements, vortex pairs from upstream rows are intensified in the downstream rows, whereas for staggered arrangements the upstream vortices are weakened.

A very interesting study in this context was provided by Liou *et al.* [77], comparing twelve different vortex generator geometries including ribs to each other. The delta-shaped vortex generator and the V-shaped ribs provided the highest heat transfer based on a constant pumping power consideration, which takes increased pressure losses into account. The delta-shaped vortex generator in this case produced only 40% of pressure loss compared to the V-shaped ribs. In an aligned arrangement the pitch between the elements was varied by Liou *et al.* [78] for pitch to vortex generator height ratios between 8 and 12. The lower pitches provided higher heat transfer at moderately increased pressure loss.

In these studies, the height of the vortex generators was smaller than the boundary layer thickness. Such vortex generators were called 'low-profile vortex generators' in the review by Lin [68], when the height is between 10% and 50% of the boundary layer thickness. These geometries were found to be efficient for boundary layer control. Also, the finlike vortex generators found on sharks or mackerels are embedded within the boundary layer with the possible function of keeping the flow attached [69].

Another interesting point arises from a study for combustor liner cooling presented by Bailey *et al.* [79]. In this study, heat transfer measurements in a rectangular cooling channel at high Reynolds numbers of 840,000 are given for a ribbed wall configuration using small height ($e/H = 0.022$) transverse ribs. The ribs enhanced heat transfer relative to the smooth channel by a factor of two. Adding an impingement arrangement upstream of the ribs enhanced heat transfer further by 40–50%.

The impinging jets introduce longitudinal vortices travelling downstream and interacting with the ribbed surface. The additionally found heat transfer enhancement can be possibly explained with this interaction of large vortex-generating structures (jets) and small scale roughness (ribs) as suggested by Garimella and Edmunds [37] for the high mass transfer capability of coral reefs.

Our current understanding on how vortices interact, how this interaction influences vortex strength and the effect of these complex situations on heat transfer is still limited. This should, and will, be a field for a lot of interesting subsequent research and will possibly combine investigations for engineering design with ecological and biological studies of natural environments.

2.5 Dimples

Systems of spherical cavities depressed in the surface (called dimples) have received increasing attention as vortex-generating elements over the last few years. The consideration of these geometries as heat transfer enhancement devices started in the mid-1980s in the former USSR [80–82] and later in the United States [83–85] and the UK [86], including detailed flow and heat transfer measurements. A good review of these developments has recently been provided by Ligrani *et al.* [8].

Dimples introduce multiple vortex pairs into the main flow, which increase heat transfer mostly outside the cavity. At the same time, they generate only a moderate pressure loss increase as they do not protrude into the flow. The vortex structures which are shed from the dimples are very complex with several vortex pairs, periodical behaviour and large scale unsteadiness as described by Ligrani *et al.* [87]. They sketched the instantaneous flow structure determined from flow visualization experiments as shown in Fig. 15 [87].

In Fig. 15, the solid line arrows indicate vortex flows above and outside the dimples, whereas the dashed line arrows denote the secondary flow within the dimple. The observed dynamic vortex pattern has been termed unstable 'self-organized', because of the unsteady-state self-oscillating behaviour. The magnitudes and frequencies of the flow oscillations depend on the dimple geometry and the flow conditions [88].

The mechanisms responsible for heat transfer enhancement were described by Ligrani *et al.* [8] as (1) shedding of multiple vortex pairs, (2) strong secondary fluid motions within the vortices, (3) shear layer reattachment within the dimple and (4) periodicity and unsteadiness in the flow.

Although the flow structure may vary considerably, it was found, that the heat transfer characteristics depend mainly on the relative dimple depth (dimple depth to dimple footprint diameter ratio δ/D) over the range of investigated Reynolds numbers. A comparison of recent results on heat transfer enhancement and pressure loss increase was given by Burgess *et al.* [89] and Burgess and Ligrani [90] for Reynolds numbers up to 80,000. For shallow dimples ($\delta/D = 0.1$) heat transfer enhancement was 1.5 with a pressure loss increase of only about 1.25 times the value for the smooth surface. Increasing the relative dimple depth to about 0.2, heat transfer enhancement increases of about 2 were determined at relative pressure loss increases between 1.5 and 2. For the deepest dimples investigated ($\delta/D = 0.3$), heat transfer increases by a factor of 2.5 compared to a smooth wall and pressure losses increased about 3 times.

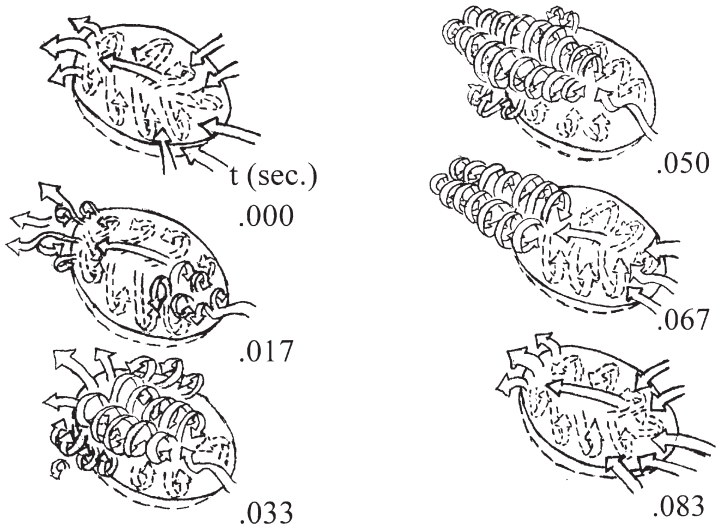

Figure 15: Sketches of instantaneous, three-dimensional flow structure in and above a dimple (from [87]).

A series of computational studies have been reported by Isaev and Leontiev [82] for different relative dimple depths. For the shallow dimples ($\delta/D < 0.22$) the flow pattern in the spherical dimple was found to be symmetric, whereas the turbulent flow past deeper dimples becomes asymmetric. These investigations revealed a 'bifurcation' of the turbulent flow with a transition from a two-cell symmetric vortex structure to an asymmetric 'tornado-like' structure. In the latter case only a single vortex may be present, which sheds from the deeper dimple at an angle close to 45°, introducing a transverse flow. This change in flow structure was related to a further increase in heat transfer. Such bi-stable vortex flow structures inside a very deep hemispherical dimple ($\delta/D = 0.5$) were also observed by Snedeker and Donaldson [91].

Most of the studies for heat transfer enhancement due to dimples concentrated on relatively narrow channels. Syred *et al.* [86] cited a heat transfer enhancement value of 2.7 in a narrow passage (channel height-to-dimple footprint diameter-ratio $H/D = 0.17$) at $\delta/D = 0.13$. Moon *et al.* [84] measured relative insensitive heat transfer distributions for the range of $0.37 < H/D < 1.49$ with enhancement values of about 2.1 at $\delta/D = 0.19$. In the investigation by Ligrani *et al.* [87] the H/D-values were varied between 0.25 and 1.0. The magnitude of flow unsteadiness was found to be more pronounced and covered larger parts of the vortex structures as H/D increases. On the other hand, Mahmood and Ligrani [92] noted that for the same range of H/D the vortex pairs, which are periodically shed from the dimple, become stronger for decreasing H/D values.

Flow instabilities occur also due to the action of centrifugal forces in boundary layers over concave curved surfaces, where they most commonly result in the generation of steady streamwise vortices. The boundary layers on convex curved walls are stabilized [93]. This leads to enhanced heat transfer for smooth concave walls and reduced heat transfer on smooth convex surfaces compared to a smooth flat wall, for turbulent flow. In view of this, Syred *et al.* [86] investigated the curvature effect for a wall containing a dimple. Flow visualization showed, that the 'tornado-like' oscillating vortices are also present for a 'curved' dimple. Similar to a smooth wall, a concave curvature increased heat transfer and a convex curvature reduced heat transfer in the dimple case (see Fig. 16). In this case the increase for a concave wall is higher than the decrease for a convex surface.

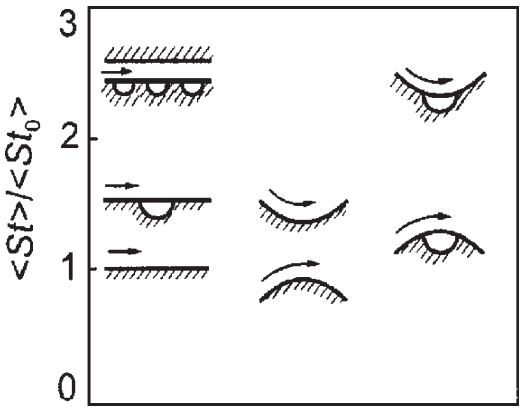

Figure 16: Average relative heat transfer rate for a single dimple on flat and curved surfaces (from [86]).

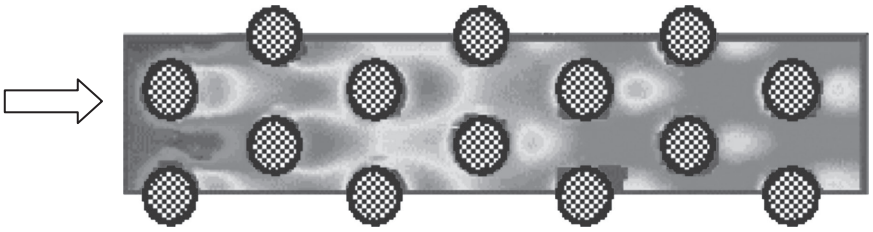

Figure 17: Heat transfer distribution on the endwall of a staggered pin-fin array (flow from left; high heat transfer—red; low heat transfer—blue).

2.6 Pin-fin heat transfer

Pin-fins or pedestals are commonly used to increase the internal heat transfer to a turbine blade or vane, especially in the trailing edge region of the blade. They increase the internal wetted surface area and the flow turbulence in the passage. The pins can be placed in various configurations. Mostly they are arranged as in-line or staggered arrays. Generally staggered arrays of pin-fins provide a higher heat transfer rate and are preferred for the cooling of gas turbine blades [94]. The heat transfer coefficient in pin arrays increases with the number of rows up to the third to fourth row and then decreases slightly towards an asymptotic value. Figure 17 shows the endwall heat transfer distribution for a staggered pin-fin array.

A good review about staggered pin-fin arrays is given by Armstrong and Winstanley [95]. They present available data on heat transfer and pressure loss for such arrangements. It can generally be said that pins are most effective for lower Reynolds numbers. For Reynolds number lower than 20,000 the enhancement in heat transfer coefficient can be of the order of 50–100%. With increasing Reynolds number the increase in heat transfer coefficient drops and reaches enhancement levels of about 10–30% above the smooth passage value for a Reynolds number of about 100,000.

More recent investigations are summarized in [8]. The importance of separating the heat transfer contributions from the endwalls and the pin-fin surface area is discussed by Chyu *et al.* [96].

Several studies consider pin-fins that differ from the circular cylindrical shape [97, 98] or the effect of endwall fillet as usually occurring due to the casting process [99].

The effect of streamwise acceleration is important for pin-fin arrays, if they are used in the converging trailing edge section of the blade. Metzger *et al.* [100] investigated this effect and proposed a correlation for the effect of flow acceleration on heat transfer.

2.7 Comparison of heat transfer enhancement techniques

For the comparison of the different passive heat transfer enhancement techniques several performance parameters can be used (see Section 1).

Han *et al.* [76] compared the measured data for delta-shaped and wedge-shaped vortex generator arrays to several rib configurations at different Reynolds number. The experimental data from this study are shown in Fig. 18. Here the heat transfer enhancement (given as Nusselt numbers relative to the Nusselt number in a smooth channel at the same Reynolds number) is shown in relationship to the friction loss increase. As can be seen, the forward, aligned configuration provides as high heat transfer as the broken V-shaped rib arrangement reaching heat transfer enhancement factors above three. The associated friction loss for these configurations is lower than for full angled or V-shaped ribs. The data shown has been taken at different Reynolds numbers. The decrease in heat transfer enhancement and, at the same time, the increase in relative pressure loss is therefore in the direction of increasing Reynolds numbers. This shows, that the optimum geometrical parameters need to be again adapted to the actual flow situation.

In a very good review paper, Ligrani *et al.* [8] collected data from a wide variety of sources and compared them using the performance criteria given by eqns (4) and (5). The results of this study are given in Figs 19 and 20. Using the performance criteria based on constant pumping power

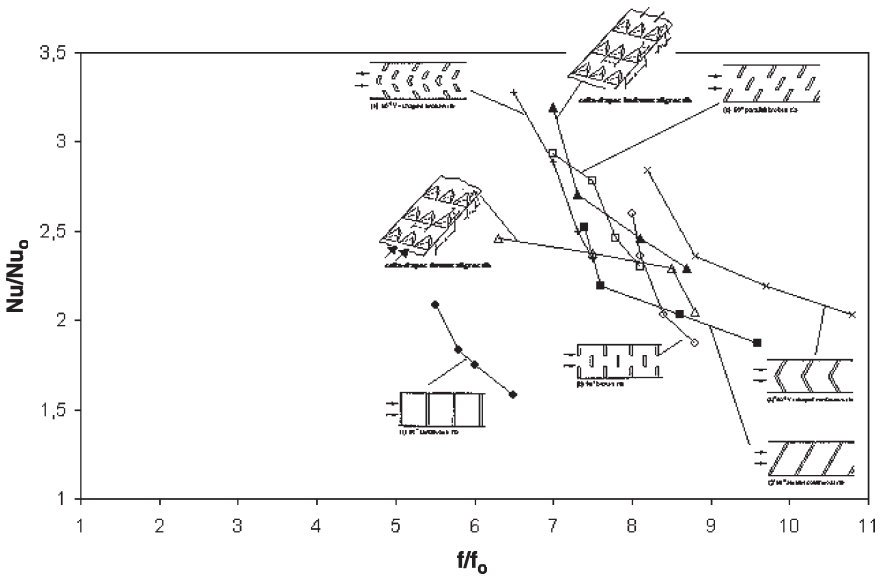

Figure 18: Heat transfer and friction factor enhancement relative to smooth channel conditions for various rib configurations and delta-shaped vortex generators (adapted from data in [76]).

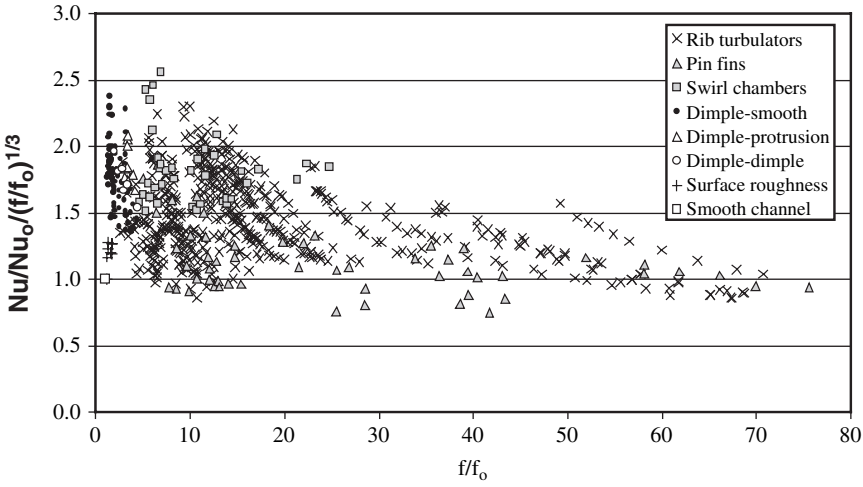

Figure 19: Comparison of different heat transfer enhancement techniques using the performance criteria based on constant pumping power (from [8]).

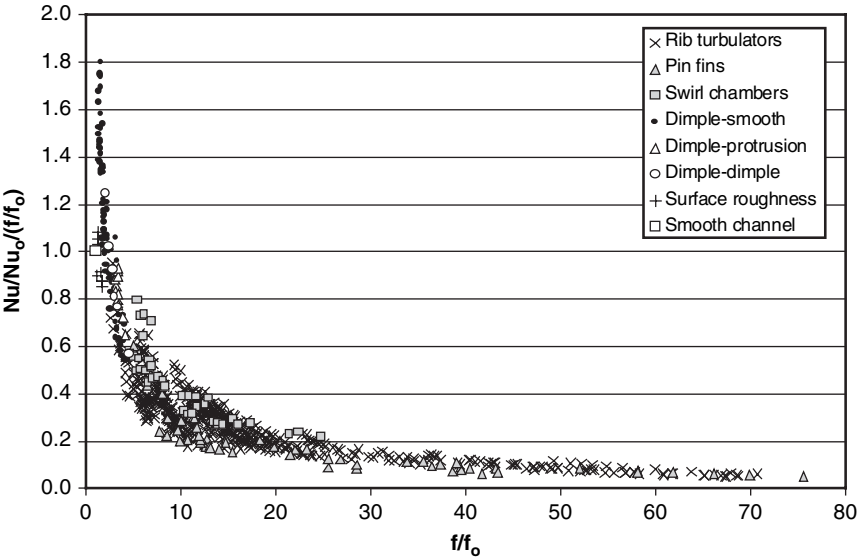

Figure 20: Comparison of different heat transfer enhancement techniques using the performance criteria based on Reynolds analogy (from [8]).

[eqn. (5)] the behaviour given in Fig. 19 is obtained. The rib turbulators are seen to enhance heat transfer with a large variation in pressure loss increase. This is related to the actual rib parameters (spacing and height) in the respective investigation. The dimple configurations are shown to give high heat transfer enhancement at relatively low pressure loss increase.

For some data points care has to be taken, since the data collected include investigations for one-sided turbulated channels and channels with turbulators on two opposite walls. This will

influence the pressure loss behaviour. The heat transfer data are usually for the wall with the heat transfer enhancement configurations.

The comparison based on the parameter derived from Reynolds analogy [eqn (4)] is given in Fig. 20. This figure effectively shows, that the data come closer together tending to an 'unique' curve. The highest values in this figure are obtained for dimpled surfaces and the lowest values are related to pin-fin arrangements. From the heat transfer enhancement view, this gives a clear advantage for dimple configurations. In a cooling application one has to keep in mind, that the high heat transfer enhancement for the dimples is related to relatively narrow channels and that dimples weaken thin walls, whereas pin-fin arrays provide additional structural strength, e.g. between the suction and pressure side walls of a turbine blade. The rib arrangements seem to be the most 'flexible' configurations, which can be adapted to local heat loads and requirements. However, several constraints have to be taken into account. Some of these considerations will be discussed next in the view of heat transfer enhancement applications for turbomachinery component cooling.

3 Applications in turbomachinery

Turbine efficiency increases with turbine inlet temperature and is limited by the allowable carrier metal temperature. Today turbines can achieve 1800–2000 K inlet temperature and 1200–1300 K carrier metal temperature for first stage components depending on their application (industrial turbines, civil aviation or military aviation). This temperature difference is achieved by active cooling and applying thermal barrier coatings. Relatively cold flow is taken from the compressor, by-passes the combustion chamber and is then used either recooled or non-recooled to achieve the required metal temperature. It is the cooling engineer's task to design a heat exchanger that efficiently and safely achieves the required thermal performance of the cooling system.

The cooling engineer performs an optimization task in a rather complex environment under many constraints, just as evolution has optimized a biological system under a set of natural constraints over thousands of years. Species that performed best survived, others, like the dinosaurs, have faded away. The engineer working in industry optimizes his system by drawing knowledge from experience as to what has worked well and what has not worked well, by analogizing from similarities available in nature and by pushing frontiers to new borders; in other words, generating 'mutations' and measuring their performance in a test environment and in the 'field' with the customers.

A large number of constraints are already present when the cooling engineer starts his optimization task, others need iteration to find improved solutions. On a global level gas turbines are used for airplane propulsion (civil or military), helicopter propulsion (civil or military) and for industrial turbines (power generation). Power generation turbines can operate either in single cycle mode or in combined cycle mode (CCPP—combined cycle power plant), meaning that downstream of the gas turbine, a steam turbine makes use of the hot gas turbine exhaust to drive a steam cycle. The steam cycle imposes for example a constraint to the range of exhaust temperatures that the gas turbine can be designed for. All systems have inherent differences that impact the design of the heat-exchanging devices.

Turbine blade and vane design for the highly thermally loaded stages of modern industrial gas turbines is the design of a heat exchanger which considers the speciality of constraints that exist in specific environments, as mentioned above. Cooling air consumption, i.e. drawing air from the compressor and bypassing the combustor to feed it back into the hollow blades that are exhibited to the hot external flow, is expensive in terms of cycle efficiency and has to be kept to a

minimal level. Assuming the general layout of a gas turbine blade, the cooling engineer has several general options to design the gas turbine blade heat exchanger:

1. Enhance the internal heat transfer coefficients and adapt the total pressure drop within the cooling system.
2. Apply a film of cold fluid close to the hot gas surface to prevent the hot gas getting to the surface.
3. Increase the blade internal heat exchanger area.
4. Apply low thermal conductivity materials, i.e. TBC (Thermal Barrier Coating), to the hot gas covered area to reduce the net heat flux into the turbine blade.
5. Use high heat capacity cooling fluid to increase the heat transfer to the cooling fluid (e.g. steam instead of air).
6. Generate a porous wall and thereby increase wall internal heat exchange area.

The large number of constraints lead to a variety of cooling systems that are used in practice. Each turbine manufacturer has developed systems that best fit his needs. A general summary of gas turbine heat transfer is included in [101] and an excellent overview over turbine cooling system design can be found in [103]. The book by Han *et al.* [56] discusses the scientific aspects of the different cooling features. In Section 2, some cooling features for heat transfer coefficient enhancement were introduced. In the remaining part of this paper, it is our intention to show some typical examples used in industry today.

The temperature response that a gas turbine blade experiences in service is a complex interaction between the external driven gas temperature (hot gas side), the external heat transfer coefficient, the metal thermal conductivity, any metal internal heat sinks, such as convective cooling channels characterized by the internal heat transfer coefficients, and the driving internal coolant temperature. Uncertainty in terms of involved parameters (e.g. radial and circumferential temperature distribution, film temperature, hot gas heat transfer coefficient, cooling air temperature, coolant heat transfer coefficient, thermal conductivity especially for TBC) lead to large uncertainties in terms of metal temperature. Lifetime sensitivity to temperature is such that 20 K uncertainty can either double or halve the predicted lifetime. Lifetime prediction is generally not done only on a straightforward analytical basis. To overcome this difficulty, laboratory and engine tests are generally performed where parameters are tested in an 'isolated' manner and part metal temperatures are measured. Statistical analysis of lifetime is a readily used tool. A very powerful tool to measure part metal temperatures is the 'thermal paint method' (e.g. [108]). This method gives metal surface temperature isotherms on locations where the high temperature paint changes colour. The metal temperature is the response of the whole thermal system and not just from the heat transfer coefficient enhancement. Thermal conductivity tends to smoothen out any peaks in heat transfer coefficient or temperature that is imposed on the metal as thermal boundary condition. To 'visualize' the individual heat transfer enhancement features and their performance, some thermal paint results will be shown below.

External secondary flow is an inevitable presence in turbomachinery. It is designed to be reduced, but still causes significant work. The passage vortex is caused by the pressure to suction side pressure difference and the horseshoe vortex due to the so-called bow wave effect in front of a vane or blade [101]. Another example is the wake of the upstream components which impact adjacent or downstream components. Therefore, strong vortical motions are present in turbine passages with associated heat transfer enhancement. This needs to be taken into account in the cooling design. A sketch of the expected secondary flows in a turbine passage is given in Fig. 21 [102].

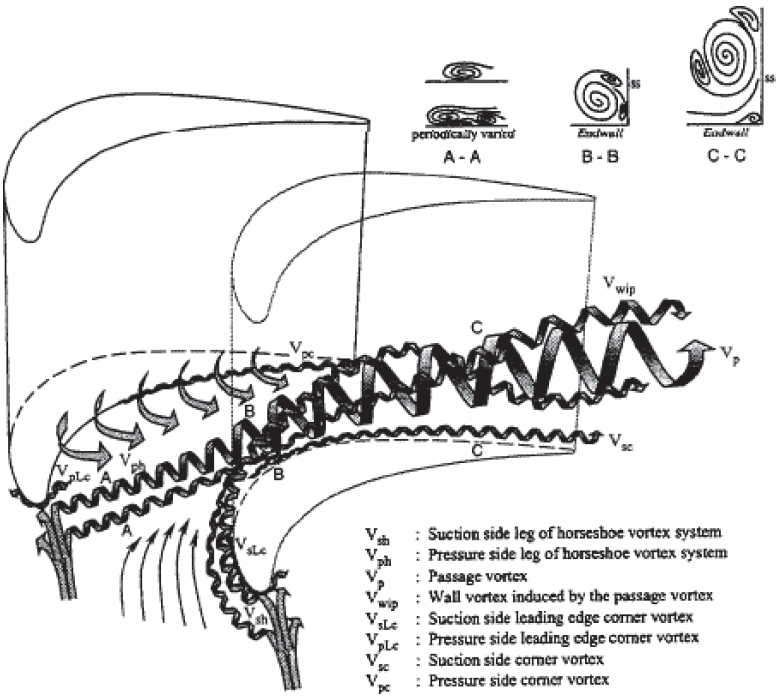

Figure 21: Secondary flow model in turbine passage (from [102]).

Due to this secondary flow field development the heat load distribution to a turbine blade will vary locally. Therefore, the cooling efficiency needs to be locally adapted. As mentioned above, heat conduction within the blade will smoothen the temperature distribution, as shown in Fig. 22 from the results of a thermal paint test. The indicated lines show the locations of isotherms on the blade surface.

Internal cooling of rotor blades is often accomplished using multipass-serpentine configurations. A discussion of the advantage of multipass systems for internal cooling is given in [103]. Multipass systems have radially aligned cooling channels and at the outer or inner boundaries the channels are connected via the so-called blade turns or bends. The heated cooling air in open systems is dumped via film cooling or trailing edge cooling into the hot gas path. Figure 23 shows an example of one such multipass cooling design [104].

The turn or bend region itself introduces secondary flow motion due to the streamline curvature. This effect is already present in the smooth channels connected by bends. A flow visualization study for such a configuration is given in Fig. 24, indicating the flow direction (2), regions of low velocity (1), areas of flow separation (3), a separation line between the introduced secondary vortices (4) and the flow attachment point (5). The special shape of the bend with the diverging outer wall is due to the adaption of the blade to the turbine annulus.

For ribbed channels, the secondary motion introduced by the turbulators will interact with the bend-induced vortices leading to the very complex flow and, therefore, heat transfer patterns. Additionally, the bends generally have a much higher pressure loss than the channels. Guide vanes can help to reduce the bend pressure loss. Thus, the heat transfer distributions will be change as shown, for example, in Fig. 25 [105].

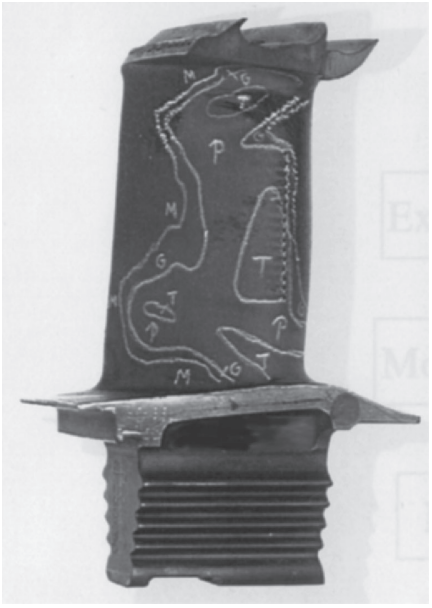

Figure 22: Isotherms on a gas turbine blade obtained from thermal paint tests (Source: Rolls Royce).

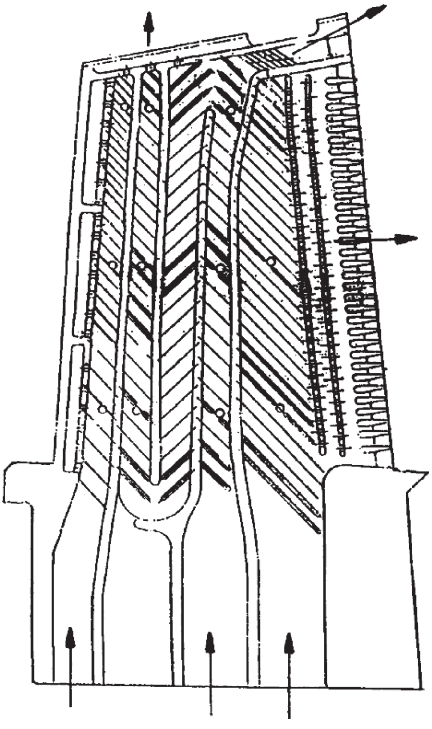

Figure 23: Cooling scheme for a rotor blade of an industrial gas turbine (from [104]).

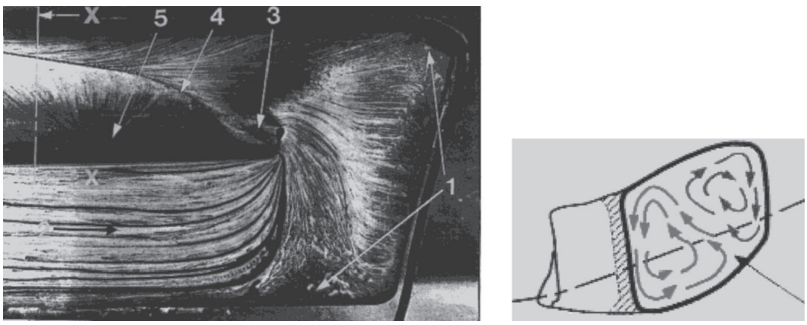

Figure 24: Flow visualization (oil painting) for a flow in a bend (left) and secondary flow in the X-X cross section (right) (from [5]).

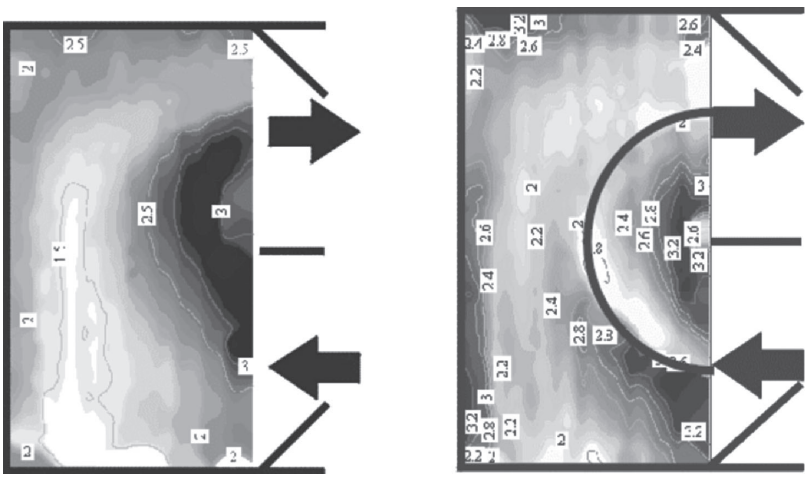

Figure 25: Heat transfer enhancement in a rectangular bend with ribbed channels. Smooth bend (left) and bend with a guide vane (right) (from [105]).

In addition, due to the first pass rib configuration and the flow turning in the bend, a strong secondary motion with associated high heat transfer is already present at the inlet to the second pass. Therefore it may be unnecessary to put ribs for heat transfer enhancement over the full length. An investigation of this aspect for a high aspect ratio two-pass cooling configuration is shown in Fig. 26. The ribs in the second pass are gradually removed and the change in heat transfer distribution is measured.

Investigating these interactions generally requires heat transfer tests modelling the full cooling circuit. Figure 27 shows a typical view of a large scale model used for such heat transfer tests together with the resulting heat transfer distribution [106]. The cooling configuration is a so-called $1 + 3$ design where the leading edge is fed with a separate channel and thereafter a three-pass system is used. A 180° guide vane is used in the bend between the first pass and the second pass, whereas a reduced 90° guide vane is applied between the second and the third passes.

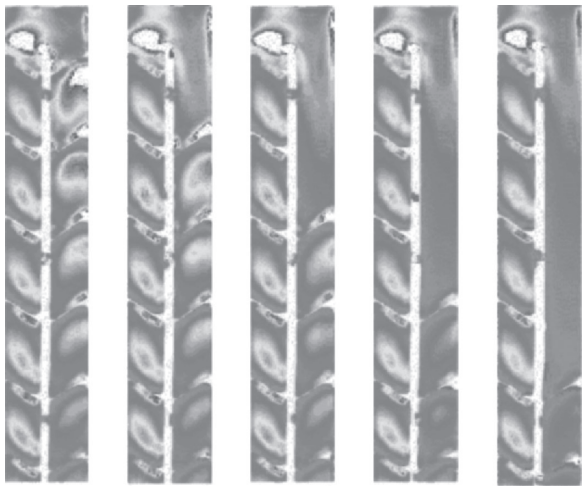

Figure 26: Heat transfer distribution in a two-pass cooling configuration with ribs. The ribs in the second pass are gradually removed from left to right.

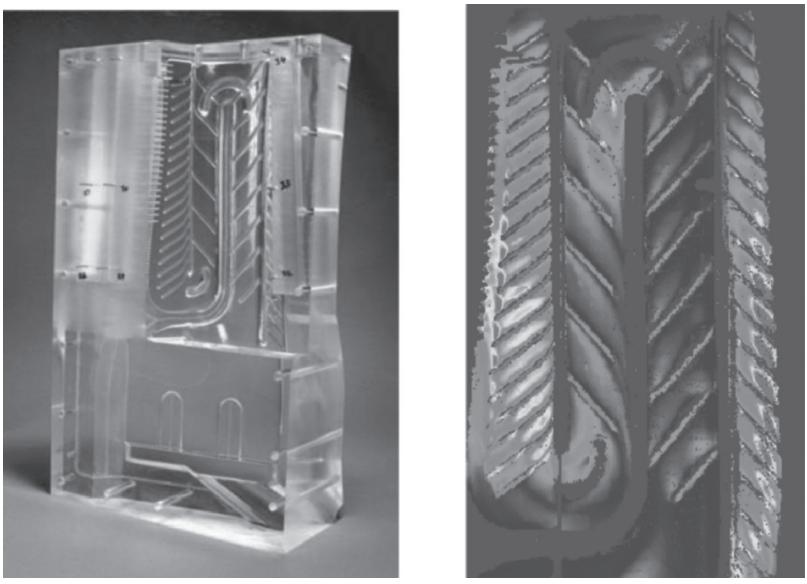

Figure 27: Large scale model (scaling factor about 5) and model test results for the heat transfer distribution inside a multipass cooling system of a gas turbine blade (from [106]).

These laboratory investigations are very helpful in detecting possible local flaws in the cooling design and provide boundary conditions for the component lifetime analysis but cannot guarantee to match all the required conditions in the real engine. Therefore, engine tests are needed to continuously improve the heat transfer designs applying, the mentioned thermal paint method to determine the component temperatures during gas turbine operation.

Figure 28: Results from a thermal paint test for the leading edge channel (right) and the first pass channel (left) of a gas turbine blade.

A typical example of the result from such tests is shown in Fig. 28 for a part of the leading edge and first pass channels from the above design. In the leading edge channel, angled shower head cooling holes are visible. They serve to reduce the high hot gas side heat load that exists at the leading edge in the stagnation region where the external boundary layer is very thin and laminar.

As mentioned above, in some applications it may be necessary to combine a heat transfer enhancement cooling feature with a mechanical design-stiffening feature. A typical configuration is one with pin-fins in the blade trailing edges. By connecting pressure and suction side walls and adding stiffness, the trailing edge opening under hot running conditions can be prevented.

When the pin-fin arrangements are fed with coolant from adjacent ribbed passages, the inlet flow to the pin-fin array is already highly disturbed (e.g. due to angled ribs in the feeding passage) and the local flow conditions may be neither in-line nor staggered. In addition, for blades, rotational effects and the consequent induced pressure distributions need to be taken into account to achieve uniform coolant distributions. These examples show that in a real design interaction of different heat transfer enhancement techniques, which can lead to improved heat transfer, characteristics as well as complex flow distributions need to be considered. The cooling designer has therefore to balance a number of different requirements, including mechanical stresses and component lifetime, turbine aerodynamics and engine performance, weight and costs, to optimize the system. A deeper understanding on how nature deals with conflicting requirements might lead to new approaches in overall design processes. Detailed knowledge of the individual phenomena, their effects on flow and heat transfer in the field of heat transfer enhancement as well as their interactions play an important role in this context.

4 Summary

Several heat transfer enhancement techniques, focussing on passive methods in single-phase forced convection processes and applications in turbomachinery component cooling have

been discussed. These techniques increase heat transfer by disturbing the fluid mechanic and thermal boundary layers, introducing flow separation and reattachment as well as a number of vortices. Although great progress has been made over the past few decades, especially with the availability of full surface measurement techniques and three-dimensional computer simulations, our detailed understanding of these complex processes is still limited. There is a strong similarity of these phenomena to natural processes such as mass transfer on rough surfaces or thermoregulation of animals, which suggests more interactive investigations between engineering and ecology or biology. This will lead to a better understanding of how nature optimizes heat (mass) transferring surfaces and could lead to more efficient thermal designs.

Acknowledgements

The authors gratefully acknowledge the permission of Elsevier for reprinting Figs 1–4 and 9 and 10, which have been published in [21, 23, 51, 52] and [71] respectively. We also acknowledge the permission of ASME for reprinting Figs 16, 21 and 27, which have been published in [86], [102] and [106] respectively. We acknowledge the permission of the American Institute of Physics for reprinting Fig. 15, which was published in [87]. We also gratefully acknowledge VDI for permission to use Fig. 23, published in [104], ROLLS-ROYCE for permission to use Fig. 22 and ALSTOM Power for permission to use Fig. 28. We gratefully acknowledge Prof. Phil Ligrani from the University of Utah for permission to use Fig. 15, which was published in [87], and for permission to use Figs 19 and 20, published in [8].

References

[1] Webb, R.L., *Principles of Enhanced Heat Transfer*, John Wiley & Sons: New York, 1993.
[2] Bergles, A.E., Some perspectives on enhanced heat transfer—second-generation heat transfer technology. *ASME Journal of Heat Transfer*, **110**, pp. 1082–1096, 1988.
[3] Bergles, A.E., Heat transfer enhancement—the encouragement of high heat fluxes. *ASME Journal of Heat Transfer*, **119**, pp. 8–19, 1997.
[4] Bergles, A.E., ExHTFT for fourth-generation heat transfer technology. *5th World Conf. on Experimental Heat Transfer, Fluid Mechanics and Thermodynamics*, Thessaloniki, 2001.
[5] Weigand, B., Semmler, K. & von Wolfersdorf, J., Heat transfer technology for internal passages of air-cooled blades for heavy-duty gas turbines. *Annals of the New York Academy of Sciences*, **934**, pp. 179–193, 2001.
[6] Weigand, B., von Wolfersdorf, J. & Neumann, S.O., Internal cooling for industrial gas turbines:Present state and novel approaches. Invited paper, *5th ISAIF*, Gdansk, Poland. ed. P. Doerffer, Internal Flows, Vol. 1, S. 67–78, IFFM Publishers, 2001.
[7] Kays, W., Crawford, M. & Weigand, B., *Convective Heat and Mass Transfer*, McGraw-Hill: New York, 2004.
[8] Ligrani, P.M., Oliveira, M.M. & Blaskovich, T., Comparison of heat transfer augmentation techniques. *AIAA Journal*, **41**, pp. 337–362, 2003.
[9] Webb, R.L., Performance evaluation criteria for use of enhanced heat transfer surfaces in heat exchanger design. *International Journal of Heat and Mass Transfer*, **24**, pp. 715–726, 1981.
[10] Raupach, M.R., Antonia, R.A. & Rajagopalan, S., Rough-wall turbulent boundary layers, *Applied Mechanical Review*, **44(1)**, pp. 1–25, 1991.

[11] Schultz, M.P., Turbulent boundary layers on surfaces covered with filamentous algae. *ASME Journal of Fluids Engineering*, **122**, pp. 357–363, 2000.
[12] Castro, I.P. & Wiggs, G.F.S., Pulsed-wire anemometry on rough surfaces, with applications to desert sand dunes. *Journal of Wind Engineering and Industrial Aerodynamics*, **52**, pp. 53–71, 1994.
[13] Dong, Z., Liu, X. & Wang, X., Aerodynamic roughness of gravel surfaces. *Geomorphology*, **43**, pp. 17–31, 2002.
[14] Commito, J.A. & Rusignuolo, B.R., Structural complexity in mussel beds: the fractal geometry of surface topography. *Journal of Experimental Marine Biology and Ecology*, **255**, pp. 133–152, 2000.
[15] Atkinson, M.J. & Bilger, R.W., Effects of water velocity on phosphate uptake in coral reef-flat communities. *Limnology and Oceanography*, **37(2)**, pp. 273–279, 1992.
[16] Nikuradse, J., Laws of flow in rough pipes. *VDI Forschungsheft*, 361, 1933.
[17] Schlichting, H., *Grenzschichttheorie*, Verlag G. Braun: Karlsruhe, 1965.
[18] Moody, L.F., Friction factors for pipe flow, *Transactions of the ASME*, **66**, p. 671, 1944.
[19] Schlichting, H., Experimentelle Untersuchungen zum Rauhigkeitsproblem. *Ingenieurs-Archiv*, **7(1)**, pp. 1–34, 1936.
[20] Clauser, F.H., Turbulent boundary layers in adverse pressure gradient. *Journal of Aeronautical Sciences*, **21**, pp. 91–108, 1954.
[21] Antonia, R.A. & Krogstad, P.A., Turbulence structure in boundary layers over different types of surface roughness. *Fluid Dynamics Research*, **28**, pp. 139–157, 2001.
[22] Krogstad, P.A. & Antonia, R.A., Surface roughness effects in turbulent boundary layers. *Experiments in Fluids*, **27**, pp. 450–460, 1999.
[23] Slanciauskas, A., Two friendly rules for the turbulent heat transfer enhancement. *International Journal of Heat and Mass Transfer*, **44**, pp. 2155–2161, 2001.
[24] Bradshaw, P., A note on 'critical roughness height' and "transitional roughness". *Physics of Fluids*, **12(6)**, pp. 1611–1614, 2000.
[25] Snyder, W.H. & Castro, I.P., The critical Reynolds number for rough-wall boundary layers. *Journal of Wind Engineering and Industrial Aerodynamics*, **90**, pp. 41–54, 2002.
[26] Bandyopadhyay, P.R., Rough-wall turbulent boundary layers in the transition regime. *Journal of Fluid Mechanics*, **180**, pp. 231–266, 1987.
[27] Jimenez, J., Turbulent flows over rough walls. *Annual Review of Fluid Mechanics*, **36**, pp. 173–196, 2004.
[28] van Rij, J.A., Belnap, B.J. & Ligrani, P.M., Analysis and experiments on three-dimensional, irregular surface roughness. *ASME Journal of Fluids Engineering*, **124**, pp. 671–677, 2002.
[29] Sigal, A. & Danberg, J.E., New correlation of roughness density effect on the turbulent boundary layer. *AIAA Journal*, **28(3)**, pp. 554–556, 1990.
[30] Bons, J.P., Taylor, R.P., McClain, S.T. & Rivir, R.B., The many faces of turbine surface roughness. *ASME Journal of Turbomachinery*, **123**, pp. 739–748, 2001.
[31] Bons, J.P., St and c_f augmentation for real turbine roughness with elevated freestream turbulence. *ASME Journal of Turbomachinery*, **124**, pp. 632–644, 2002.
[32] Belnap, B.J., van Rij, J.A. & Ligrani, P.M., A Reynolds analogy for real component surface roughness. *International Journal of Heat and Mass Transfer*, **45**, pp. 3089–3099, 2002.
[33] Bilger, R.W. & Atkinson, M.J., Anomalous mass transfer of phosphate on coral reef flats. *Limnology and Oceanography*, **37(2)**, pp. 261–272, 1992.

[34] Helmuth, B.S.T., Sebens, K.P. & Daniel, T.L., Morphological variation in coral aggregations: branch spacing and mass flux to coral tissues. *Journal of Experimental Marine Biology and Ecology*, **209**, pp. 233–259, 1997.
[35] Thomas, F.I.M. & Atkinson, M.J., Ammonia uptake by coral reefs: Effects of water velocity and surface roughness on mass transfer. *Limnology and Oceanography*, **42(1)**, pp. 81–88, 1997.
[36] Patterson, M.R., Sebens, K.P. & Olson, R.R., *In situ* measurements of flow effects on primary production and dark respirations in reef corals. *Limnology and Oceanography*, **36(5)**, pp. 936–948, 1991.
[37] Gardella, D.J. & Edmunds, P.J., The effect of flow and morphology on boundary layers in the scleractinians *Dichocoenia stokesii* (Milne-Edwards and Haime) and *Stephanocoenia michilini* (Milne-Edwards and Haime). *Journal of Experimental Marine Biology and Ecology*, **256**, pp. 279–289, 2001.
[38] Shashar, N., Kinane, S., Jokiel, P.L. & Patterson, M.R., Hydromechanical boundary layers over a coral reef. *Journal of Experimental Marine Biology and Ecology*, **199**, pp. 17–28, 1996.
[39] Dipprey, D.F. & Sabersky, R.H., Heat and momentum transfer in smooth and rough tubes at various Prandtl numbers. *International Journal of Heat and Mass Transfer*, **6**, pp. 329–353, 1963.
[40] Baird, M.E. & Atkinson, M.J., Measurement and prediction of mass transfer to experimental coral reef communities. *Limnology and Oceanography*, **42(8)**, pp. 1685–1693, 1997.
[41] Nowell, A.R.M. & Jumars, P.A., Flow environments of aquatic benthos. *Annual Reviews Ecological Systems*, **15**, pp. 303–328, 1984.
[42] Patel, V.C., Perspective: flow at high reynolds number and over rough surfaces—achilles heel of CFD. *ASME Journal of Fluids Engineering*, **120**, pp. 434–444, 1998.
[43] Cui, J., Patel, V.C. & Lin, C.L., Predictions of turbulent flow over rough surfaces using a force field in large eddy simulation. *ASME Journal of Fluids Engineering*, **125**, pp. 2–9, 2003.
[44] Wang, Z.J., Chi, X.K., Shih, T. & Bons, J., Direct simulation of surface roughness effects with RANS and DES approaches on viscous adaptive Cartesian grids, *AIAA-2004-2420*, 2004.
[45] Dalle Donne, M. & Meyer, L., Turbulent convective heat transfer from rough surfaces with two-dimensional rectangular ribs. *International Journal of Heat and Mass Transfer*, **20**, pp. 583–620, 1977.
[46] Meyer, L., Thermohydraulic characteristics of single rods with three-dimensional roughness. *International Journal of Heat and Mass Transfer*, **17**, pp. 1043–1058, 1982.
[47] Sheriff, N. & Gumley, P., Heat-transfer and friction properties of surfaces with discrete roughness. *International Journal of Heat and Mass Transfer*, **9**, pp. 1297–1320, 1966.
[48] Nunner, W., VDI Forschungsheft 455, B22:5, 1956.
[49] Kader, B.A. & Yaglom, A.M., Turbulent heat and mass transfer from a wall with parallel roughness ridges. *International Journal of Heat and Mass Transfer*, **20**, pp. 345–357, 1977.
[50] Dawson, D.A. & Trass, O., Mass transfer at rough surfaces. *International Journal of Heat and Mass Transfer*, **15**, pp. 1317–1336, 1972.
[51] Berger, F.P. & Hau, F.L., Local mass/heat transfer distributions on surfaces roughened with small square ribs. *International Journal of Heat and Mass Transfer*, **22**, pp. 1645–1656, 1979.

[52] Webb, R.L., Eckert, E.R.G. & Goldstein, R.J., Heat transfer and friction in tubes with repeated-rib roughness. *International Journal of Heat and Mass Transfer*, **14**, pp. 601–617, 1971.
[53] Han, J.C., Glicksman, L.R. & Rohsenow, W.M., An investigation of heat transfer and friction for rib-roughened surfaces. *International Journal of Heat and Mass Transfer*, **21**, pp. 1143–1156, 1978.
[54] Han, J.C. & Dutta, S., Internal Convection Heat Transfer and Cooling: An Experimental Approach, VKI-LS 1995-05, Heat Transfer and Cooling in Gas Turbines, 1995.
[55] Taslim, M.E., Convective cooling in non-rotating and rotating channels—experimental aspects, *Aero-thermal Performance of Internal Cooling Systems in Turbomachines*, VKI-LS 2000-03, 2000.
[56] Han, J.C., Dutta, S. & Ekkad, S.V., *Gas Turbine Heat Transfer and Cooling Technology*, Taylor & Francis Publishers, 2001.
[57] Han, J.C., Zhang, Y.M. & Lee, C.P., Augmented heat transfer in square channels with parallel, crossed and V-shaped angled ribs. *ASME Journal of Heat Transfer*, **113**, pp. 590–596, 1991.
[58] Han, J.C. & Zhang, Y.M., High performance heat transfer ducts with parallel broken and V-shaped broken ribs. *International Journal of Heat and Mass Transfer*, **35**, pp. 513–523, 1992.
[59] Weigand, B., What should we measure? The industrial—engine heat transfer perspective. *Proc. of the XIV Bi-annual Symp. On Measuring Techniques in Transonic and Supersonic Flow in Cascades and Turbomachines*. Invited Lecture. Limerick: Ireland, 1998.
[60] Zhang, Y.M., Gu, W.Z. & Han, J.C., Heat transfer and friction in rectangular channels with ribbed or ribbed-grooved walls. *ASME Journal of Heat Transfer*, **116**, pp. 58–65, 1994.
[61] Wright, L.M., Fu, W.L. & Han, J.C., Thermal performance of angled, v-shaped and w-shaped rib turbulators in rotating rectangular cooling channels. *Proc. of the Int. Gas Turbine Conference*, Vienna, Austria, *ASME GT2004-54073*, 2004.
[62] Rhee, D.H., Lee, D.H. & Cho, H.H., Effects of duct aspect ratio on heat/mass transfer with discrete V-shaped ribs. *Proc. of the Int. Gas Turbine Conference*, Atlanta, USA, *ASME GT2003-38622*, 2003.
[63] Hall, K., Johnson, B., Weigand, B. & Wu, P.S., Coolable Blade. United States Patent, Patent No. 5919031, 1999.
[64] Beeck, A., Johnson, B., Weigand, B. & Wu, P.S., Cooling system for the leading edge of a hollow blade for a gas turbine, European Patent, EP0892149, 1997.
[65] Stroock, A.D., Dertinger, S.K.W., Ajdari, A., Mezic, I., Stome, H.A. & Whitesides, G.M., Chaotic mixer for microchannels. *Science*, **295**, pp. 647–651, 2002.
[66] Hong, S., Thiffeault, J.-L., Frechette, L. & Modi, V., Numerical study of mixing in microchannels with patterned zeta potential surfaces. *Proc. of IMECE'03*, Washington D.C., November 16–21, IMECE2003-41912, 2003.
[67] Schubauer, G.B. & Spangenberg, W.G., Forced mixing in boundary layers. *Journal of Fluid Mechanics*, **8**, pp. 10–32, 1960.
[68] Lin, J.C., Review of research on low-profile vortex generators to control boundary layer separation. *Progress in Aerospace Sciences*, **38**, pp. 389–420, 2002.
[69] Bechert, D.W., Bruse, M., Hage, W. & Meyer, R., Fluid mechanics of biological surfaces and their technological application. *Naturwissenschaften*, **87**, pp. 157–171, 2000.
[70] Meagher, E.M., McLellan, W.A., Westgate, A.J., Wells, R.S., Frierson, Jr., D. & Pabst, D.A., The relationship between heat flow and vasculature in the dorsal fin of

wild bottlenose dolphins *Tursiops truncates*. *Journal of Experimental Biology*, **205**, pp. 3475–3486, 2002.

[71] Jacobi, A.M. & Shah, R.K., Heat transfer surface enhancement trough the use of longitudinal vortices: a review of recent progress. *Experimental Thermal and Fluid Science*, **11**, pp. 295–309, 1995.

[72] Fiebig, M., Vortices, generators and heat transfer. *Trans. IChemE Part A*, **76**, pp. 108–122, 1998.

[73] Fiebig, M., Embedded vortices in internal flow: heat transfer and pressure loss enhancement. *International Journal of Heat and Fluid Flow*, **16**, pp. 376–388, 1995.

[74] Torii, K., Kwak, K.M. & Nishino, K., Heat transfer enhancement accompanying pressure loss reduction with winglet-type vortex generators for fin-tube heat exchangers, *International Journal of Heat and Mass Transfer*, **45**, pp. 3795–3801, 2002.

[75] Chen, Y., Fiebig, M. & Mitra, N.K., Conjugate heat transfer of a finned oval tube with a punched longitudinal vortex generator in form of a delta winglet—parametric investigations of the winglet. *International Journal of Heat and Mass Transfer*, **41**, pp. 3961–3978, 1998.

[76] Han, J.C., Huang, J.J. & Pang Lee, C., Augmented heat transfer in square channels with wedge-shaped and delta-shaped turbulence promoters. *Journal of Enhanced Heat Transfer*, **1(1)**, pp. 37–52, 1993.

[77] Liou, T.M., Chen, C.C. & Tsai, T.W., Heat transfer and fluid flow in a square duct with 12 different shaped vortex generators. *ASME Journal of Heat Transfer*, **122**, pp. 327–335, 2000.

[78] Liou, T.M., Tsai, T.W. & Chen, C.C., Liquid crystal visualizations and measurements of heat transfer in a square duct with different pitches of vortex generator arrays. *Journal of Flow Visualization & Image Processing*, **5**, pp. 295–308, 1998.

[79] Bailey, J.C., Nirmalan, N.V., Bunker, R.S., Intile, J., Fric, T.F. & Tolpadi, A.K., Experimental and numerical study of heat transfer in a gas turbine combustor liner. *ASME GT-2002-30183*, 2002.

[80] Afanasyev, V.N., Chudnovsky, Ya.P., Leontiev, A.I. & Roganov, P.S., Turbulent flow friction and heat transfer characteristics for spherical cavities on a flat plate. *Experimental Thermal and Fluid Science*, **7**, pp. 1–8, 1993.

[81] Shchukin, A.V., Kozlov, A.P. & Agachev, R.S., Study and application of hemispheric cavities for heat transfer augmentation. *ASME 95-GT-59*, 1995.

[82] Isayev, S.A. & Leontiev, A.I., Numerical simulation of vortex enhancement of heat transfer under conditions of turbulent flow past a spherical dimple on the wall of a narrow channel. *High Temperature*, **41(5)**, pp. 755–770, 2003.

[83] Chyu, M.K., Yu, Y., Ding, H., Downs, J.P. & Soechting, F.O., Concavity enhanced heat transfer in an internal cooling passage. *ASME 97-GT-43*, 1997.

[84] Moon, H.K., O'Connell, T. & Glezer, B., Channel height effect on heat transfer and friction in a dimpled passage. *ASME Journal of Engineering Gas Turbine and Power*, **122**, pp. 307–313, 2000.

[85] Mahmood, G.I., Hill, M.L., Nelson, D.L., Ligrani, P.M., Moon, H.K. & Glezer, B., Local heat transfer and flow structure on and above a dimpled surface in a channel. *ASME Journal of Turbomachinery*, **123**, pp. 115–123, 2003.

[86] Syred, N., Khalatov, A., Kozlov, A., Shchukin, A. & Agachev, R., Effect of surface curvature on heat transfer and hydrodynamics within a single hemispherical dimple. *ASME Journal of Turbomachinery*, **123**, pp. 609–613, 2001.

[87] Ligrani, P.M., Harrison, J.L., Mahmood, G.I. & Hill, M.L., Flow structure due to dimple depressions on a channel surface. *Physics of Fluids*, **13(11)**, pp. 3442–3451, 2001.
[88] Terekhov, V.I., Kalinina, S.V. & Mshvidobadze, Yu.M., Heat transfer coefficient and aerodynamic resistance on a surface with a single dimple. *Journal of Enhanced Heat Transfer*, **4**, pp. 131–145, 1997.
[89] Burgess, N.K., Oliveira, M.M. & Ligrani, P.M., Nusselt number behavior on deep dimple surfaces within a channel. *ASME Journal of Heat Transfer*, **125**, pp. 11–18, 2003.
[90] Burgess, N.K. & Ligrani, P.M., Effects of dimple depth on Nusselt numbers and friction factors for internal cooling in a channel. *Proc. of the Int. Gas Turbine Conference*, Vienna, Austria, *ASME GT2004-54232*, 2004.
[91] Snedeker, R.S. & Donaldson, C.P., Observation of a bistable flow in a hemispherical cavity. *AIAA Journal*, **4(4)**, pp. 735–736, 1966.
[92] Mahmood, G.I. & Ligrani, P.M., Heat transfer in a dimpled channel: combined influences of aspect ratio, temperature ratio, Reynolds number, and flow structure. *International Journal Heat and Mass Transfer*, **45**, pp. 2011–2020, 2002.
[93] Saric, W.S., Görtler vortices. *Annual Review of Fluid Mechanics*, **26**, pp. 379–409, 1994.
[94] Sparrow, E.M., Ramsey, J.W. & Altemani, C.A.C., Experiments on in-line pin fin arrays and performance comparisons with staggered array. *ASME Journal of Heat Transfer*, **102**, pp. 44–50, 1980.
[95] Armstrong, J. & Winstanley, D., A review of staggered array pin fin heat transfer for turbine cooling applications. *ASME Journal of Turbomachinery*, **110**, pp. 94–103, 1988.
[96] Chyu, M.K., Hsing, Y.C., Shih, T.I.-P. & Natarajan, V., Heat transfer contributions of pins and endwall in pin–fin arrays. *ASME Journal of Turbomachinery*, **121**, pp. 257–263, 1999.
[97] Chyu, M.K., Hsing, Y.C. & Natarajan, V., Convective heat transfer of cubic fin arrays in a narrow channel. *ASME Journal of Turbomachinery*, **120**, pp. 362–367, 1998.
[98] Uzol, O. & Camci, C., Elliptical pin fins as an alternative to circular pin fins for gas turbine blade cooling applications. Part 1: Endwall heat transfer and total pressure loss characteristics. *ASME 2001-GT-232*, 2001.
[99] Chyu, M.K., Heat transfer and pressure drop for short pin-fin arrays with pin-endwall fillet. *ASME Journal of Heat Transfer*, **112**, pp. 926–932, 1990.
[100] Metzger, D.E., Shepard, W.B. & Haley, S.W., Row resolved heat transfer variation in pin fin arrays including the effects of non-uniform arrays and flow convergence. *ASME 86-GT-132*, 1986.
[101] Lakshminarayana, B., *Fluid Dynamics and Heat Transfer of Turbomachinery*, John Wiley & Sons: New York, 1996.
[102] Wang, H.P., Olson, S.J., Goldstein, R.J. & Eckert, E.R.G., Flow visualisation in a linear turbine cascade of high performance turbine blades. *ASME 95-GT-7*, 1995.
[103] Daily, D., Design and calculation issues. *Aero-thermal Performance of Internal Cooling Systems in Turbomachines*, VKI-LS 2000-03, 2000.
[104] Schulenberg, T., Kopper, F. & Richardson, J., An advanced blade design for V84.3 gas turbines. *VDI Berichte*, **1185**, pp. 257–275, 1995,
[105] Schnieder, M., Höcker, R. & von Wolfersdorf, J., Heat transfer and pressure loss in a 180°-turn of a rectangular, rib-roughened two passage channel. *5th World Conf. on Experimental Heat Transfer, Fluid Mechanics and Thermodynamics*, ExHFT5, Thessaloniki, 2001.
[106] Jennions, I.K., Sommer, T., Weigand, B. & Aigner, M., The GT24/26 low pressure turbine, *ASME 98-GT-29*, 1998.

[107] Amro, M., PhD Thesis, Institute of Aerospace Thermodynamics (ITLR), University of Stuttgart, 2004.
[108] Gregg, S.G., Heidegger, N.J. & Mikkelson, R.A., Computational modeling and thermal paint verification of film-cooling designs for an unshrouded high-pressure turbine blade. *ASME 99-GT-330*, 1999.
[109] von Wolfersdorf, J., Ott, P. & Weigand, B., Temperature and pressure sensitive coatings. *Flow Phenomena in Nature*, Vol. 1, pp. 747–766, 2006.
[110] Weigand, B. & Simon, V., Laws of similarity in fluid mechanics. *Flow Phenomena in Nature*, Vol. 1, pp. 20–35, 2006.